Sugar assimilation underlying dietary evolution of Neotropical bats

Andrea Bernal-Rivera[1,2 †], Jasmin Camacho[1], Sofia Robb[1], Jonathon Russell[1], Kexi Yi[1], Yongfu Wang[1], Dai Tsuchiya[1], Oscar E. Murillo-García[2 *], Nicolas Rohner[1,3 *]

[1] Stowers Institute for Medical Research, Kansas City, MO 64110, USA.

[2] Grupo de Investigación en Ecología Animal, Departamento de Biología, Universidad del Valle, Cali 76001, Colombia.

[3]Department of Molecular and Integrative Physiology, University of Kansas Medical Center, Kansas City, Kansas, USA

† these authors contributed equally

* Correspondence: nro@stowers.org; oscar.murillo@correounivalle.edu.co

Highlights

- Sugar assimilation differences emphasize metabolic adaptations to diet
- Glucose tolerance tests provide a quick and practical assessment of dietary ecology
- Bat genomes exhibit positive selection on digestive enzymes and glucose transporters
- Glucose absorption differences can be explained by gut anatomy
- Extreme blood glucose (>650 mg/dL) coincides with constitutive expression of apical *Slc2a2*
- The regulation of *Sglt1* and apical *Slc2a2* highlights differences in blood glucose levels

Summary

Specializations in animal diets drive selective demands on morphology, anatomy, and physiology. Studying adaptations linked to diet evolution benefits from examining Neotropical bats, a remarkable group with high taxonomic and trophic diversity. In this study we performed glucose tolerance tests on wild-caught bats, which revealed distinct responses to three sugars present in different foods: trehalose (insects), sucrose and glucose (fruits and nectar). Insect eating bats responded most strongly to trehalose, while bats with nectar and fruit-based diets exhibited heightened response to glucose and sucrose, reaching blood sugar levels over 600 mg/dL. To reveal positive selection in sugar assimilation genes we performed genome analysis of 22 focal bat species and 2 outgroup species. We identified selection in the ancestral vespertilionid branch (insect-eaters) for the digestive enzyme Trehalase, while sucrase-isomaltase exhibited selection in branches leading to omnivorous and nectar diets. Unexpectedly, the insect-eating lineage *Myotis* exhibited sucrase-isomaltase selection, potentially explaining their heightened sucrose assimilation. Furthermore, the glucose transporters SLC2A3 and SLC2A2 showed selection in lineages associated with nectar and blood diets. By examining cellular features of the small intestine, we discovered that sugar consumption strongly impacted numerous digestive traits, providing valuable insight into the physiological implications of the identified molecular adaptations. To elucidate this further, we used HCR RNA-FISH to perform single molecule *ex vivo* gene expression analysis of enterocyte response to a glucose meal in three focal species. We observed unusually high activity in the glucose transporter *Slc2a2* during the fasted state of nectar bats that did not change upon feeding. Comparatively, nectar bats exhibited an enhanced capacity for intestinal absorption of dietary sugar primarily through *Slc2a2*, while fruit bats relied on increasing

levels of *Slc5a1*. Overall, this study highlights the intricate interplay between molecular, morphological, and physiological aspects of diet evolution and provides new insights to our understanding of sugar assimilation mechanisms in mammals.

Key words: chiroptera, dietary evolution, blood glucose, hyperglycemia, metabolism, GLUT2, SGLT1.

Graphical Abstract

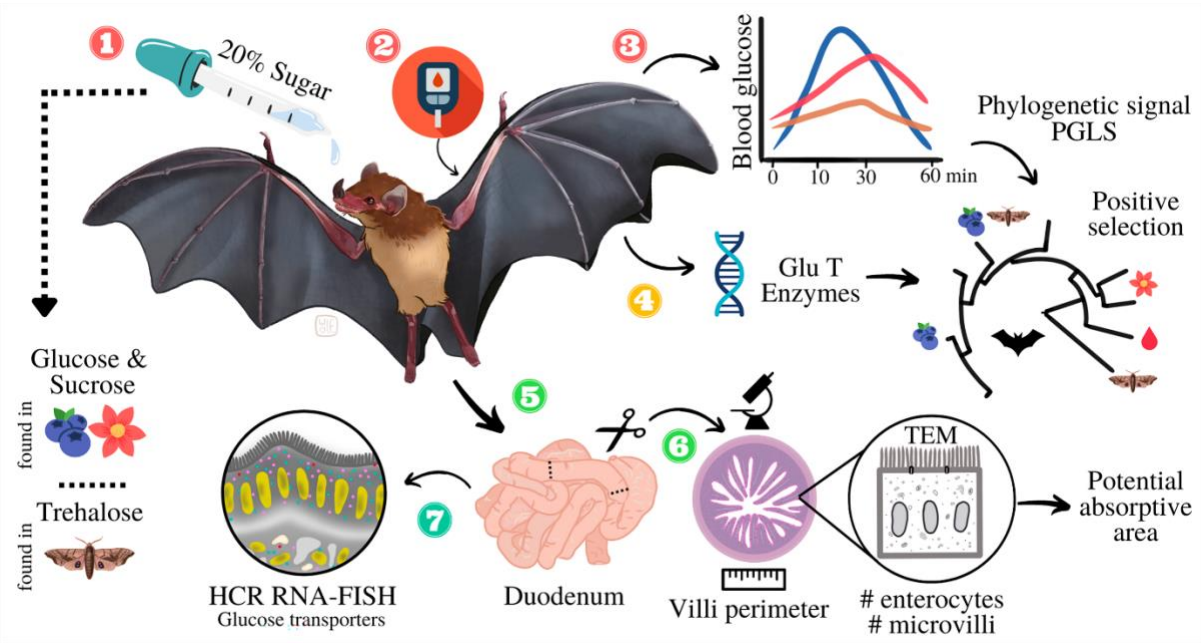

Results and Discussion

<u>*In vivo* physiology</u>

Among mammals, bats offer a unique opportunity to investigate metabolic adaptations due to their wide variety of diets. They have specialized from an ancestor with an insect-heavy diet to fruit, nectar, meat, blood, and other food sources (Neuweiler, 2000). To assess metabolic adaptations related to dietary diversification, we focused on the glucose homeostasis pathway, which directly regulates glucose energy during and between food intake and is vital for long-term health and survival. We performed *in vivo* oral glucose tolerance tests on 194 wild-caught bats from 27 species (Supplemental Table 1) to assess their ability to process three dietary sugars (Wyatt & Kalf, 1957; Baker et al., 1998): trehalose (formed by two glucose molecules), sucrose (formed by glucose and fructose), and glucose. The bats were fasted for 10-12 hours, and blood glucose levels were measured before and after consuming a single sugar (5.4g/kg, Kelm et al., 2011). Measurements were taken at 10, 30, and 60 minutes post-ingestion, revealing distinct patterns in the rise and fall of blood glucose levels between diets (Fig. 1A). To better quantify physiological responses we classified them into four patterns: *"Fast"*, *"Medium"*, *"Slow"*, and *"Limited"* (Fig. 1B), based on the speed and extent of assimilation (see Methods 1.2.1).

In insectivorous and omnivorous bats, we observed <u>trehalose</u> assimilation with blood glucose levels reaching up to 160 mg/dL with a *"Slow"* tolerance curve indicating glucose absorption continuing until 60 minutes. In contrast, bats with nectar and fruit diets exhibited a *"Limited"* ability to assimilate trehalose, showing blood glucose levels remaining within a narrow range and only rising to 60 mg/dL. These findings align with existing evidence that the trehalase gene (*treh*) is non-functional in non-insectivorous bats (Schondube et al., 2001; Jiao et al., 2019). Interestingly, individuals of the vampire

bat showed a slight rise and fall in blood glucose levels following trehalose consumption, reaching levels of 90 mg/dL. We propose that the minor elevation in blood glucose levels in non-insectivorous bats could be attributed to the activity of the gut microbiome (Zepeda Mendoza et al., 2018; Ingala et al., 2021) or use of energetic reserves.

When tested for sucrose, insect-feeding bats showed a gradual increase in blood glucose levels 30 minutes after sucrose ingestion, except for *Myotis*, which surprisingly showed a rapid rise to 200 mg/dL within 10 minutes, followed by a decline to 140 mg/dL at 60 minutes, indicating a "*Medium*" sucrose assimilation. This suggests that *Myotis* digests sucrose more efficiently than trehalose despite its classification as an insect-feeder. As expected, the vampire bats showed *"Limited"* sucrose assimilation, with blood glucose levels remaining below 96 mg/dL throughout the experiment. Among omnivores, *Carollia* levels peaked at 10 min (200 mg/dL) and gradually declined, whereas *Phyllostomus* had a lower peak at 10 min (100 mg/dL), and slowly decreased. These patterns reflect the varying degrees of omnivory, where *Carollia* mainly feed on piper fruits and some insects while *Phyllostomus* consume insects, fruits, small vertebrates, flowers, nectar and pollen (Santos et al., 2003; York & Billings, 2009). Fruit and nectar bats exhibited two major responses to sucrose: 1. "*Fast"* assimilation with rapid rise in blood glucose (200mg/dl) within 10 minutes and subsequent rapid decrease to basal levels after 60 min for *Artibeus*, *Dermanura*, and *Choeroniscus*; 2. "*Medium"* assimilation with a slow increase, reaching a maximum after 30 minutes (300 mg/dL) for *Sturnira*, *Uroderma*, and *Glossophaga*. These findings highlight significative variations in sucrose assimilation among bats with different diets, as well as within species of the same dietary category, indicating the diversification of disaccharide assimilation.

When tested for glucose ingestion we observed higher blood glucose levels across all bat species compared to trehalose and sucrose feedings. Bats with insect, meat, and blood diets showed a gradual increase in blood glucose levels and stayed below 300 mg/dL, except in *Pteronotus* (> 350 mg/dL), but still indicating a *"Slow"* assimilation pattern. Among omnivorous bats, *Carollia* reached a peak of 423 mg/dL at 10 minutes and rapidly decreased levels until 60 minutes, while *Phyllostomus*, reached a peak of 225 mg/dL at 30 minutes and then declined by 60 minutes. Bats with fruit diets exhibited the most extreme rise and fall of blood glucose levels, with levels reaching up to 600 mg/dL within 10 minutes in *Artibeus* and *Dermanura*, and levels dropping to 100 mg/dL in some individuals after 60 minutes. This *"Fast"* assimilation curve is likely due to an enhanced insulin sensitivity in these species (Protzek et al., 2010). Other fruit bats showed high glucose levels within 30 minutes, with *Uroderma* reaching 476 mg/dL and *Sturnira* reaching 357 mg/dL, followed by a subsequent decrease. In nectarivores, we observed *"Fast"* assimilation curves, with *Glossophaga* again reaching levels above the detection limit of 600 mg/dL at 10 minutes and *Choeroniscus* reaching 300 mg/dL at the 10 minutes timepoint, which is probably related to differences in plant/nectar preferences and availability for each species (Ayala-Berdon et al., 2013; Ortega-García et al., 2022). These readings of more than 600mg/dL are, to our knowledge, the highest documented for any wild species feeding on a single sugar dose. In contrast, captive *Glossophaga soricina* individuals reached a peak of 360 mg/dL after 30 minutes when fed with a similar single dose (Kelm et al., 2011) and did not exceed 470 mg/dL even when fed a higher glucose dose (9 g/kg). Nectar bats exhibited a slower decline in blood glucose levels compared to fruit bats, consistent with recent studies that found no plasma insulin response to feeding in nectar-bats at rest, and proposed an exercise-mediated regulatation of glucose homeostasis (Welch et al., 2007; Welch & Chen, 2014; Kelm et al., 2011; Peng et al., 2017; Castro et al., 2021). These findings highlight how sugar assimilation capability in Neotropical bats reflect their natural food preferences, raising questions about how bats with different diets can absorb and compensate for variations in circulating blood glucose.

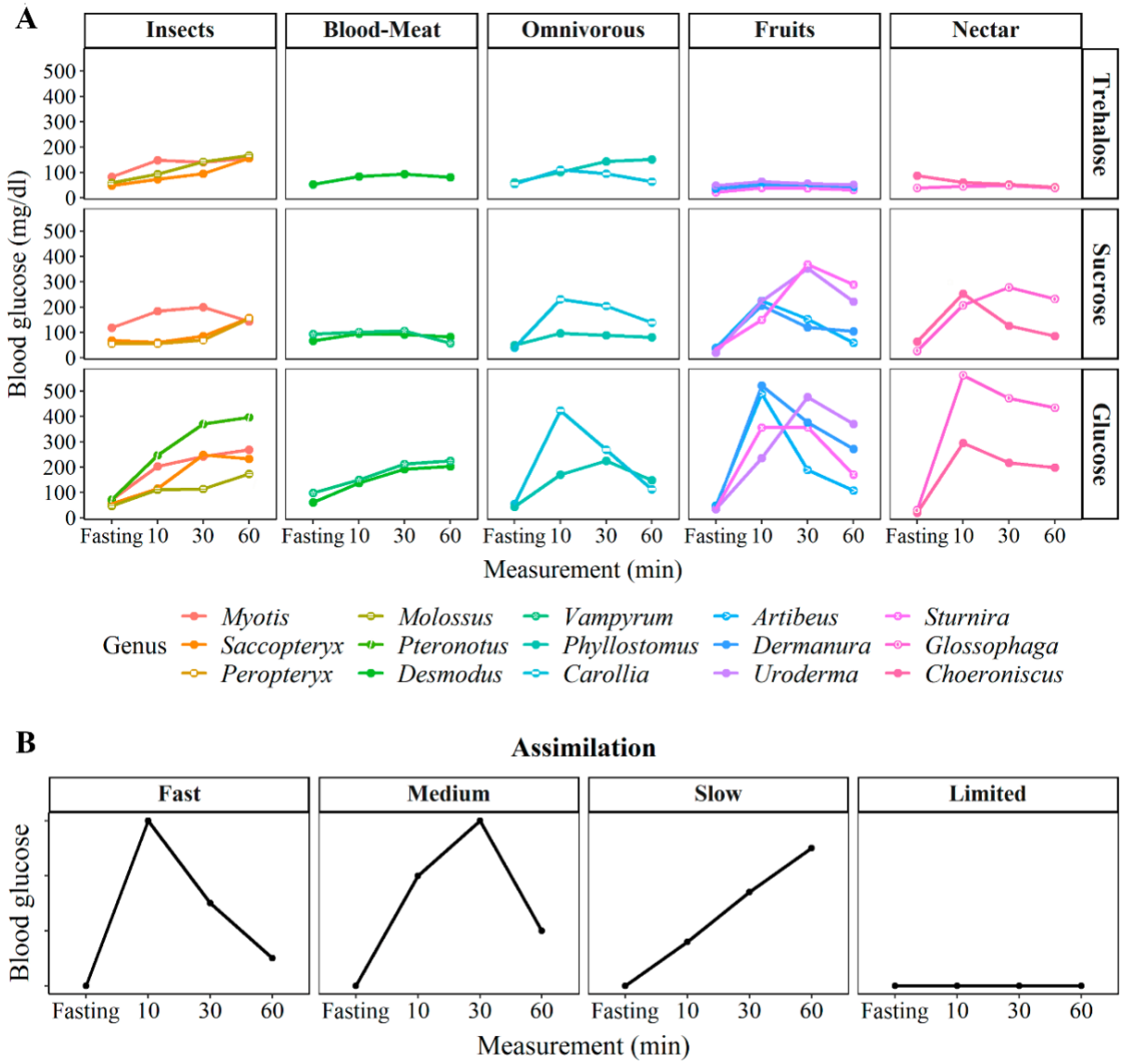

Fig. 1. A. Average assimilation curves for trehalose, sucrose, and glucose among Neotropical bats with different food preferences: insects, blood or meat, mixed (omnivorous), fruits, and nectar. The sample size varied among genera from 1 to 52 individuals (Supplemental Table 1). B. General curves to describe the temporal pattern of sugar assimilation.

To evaluate the impact of evolutionary history on sugar assimilation, we employed Pagel's λ (Pagel, 1999) to test the phylogenetic signal for each assimilation pattern. For sucrose, we obtained a λ value of 0.93, while for trehalose it was 0.99 (Supplemental information Table 2A). However, glucose did not show a phylogenetic signal. These results suggest that glucose assimilation patterns are not influenced by phylogenetic relationships, whereas assimilation of disaccharides may be mediated by mechanisms that are more consistent among phylogenetically related species. Additionally, we fitted Phylogenetic Generalized Least Squares (PGLS) with a Brownian motion (BM) evolutionary model (Symonds & Blomberg, 2014) to compare adaptations in blood glucose homeostasis while controlling for phylogenetic relatedness. The best-supported model included the effect of diet ($p<0.05$), indicating a strong association between the assimilation patterns and dietary preferences (Supplemental information Table 2B).

Molecular adaptations related to sugar assimilation

To identify molecular adaptations underlying the association between sugar assimilation and different diets, we tested for positive selection in 22 bat genomes from species represented in our *in vivo* data, along with two outgroup species (Supplemental Table 4, 5). We focused on genes involved in glucose transport and absorption, crucial for regulating blood glucose levels and facilitating glucose uptake into cells (Supplemental Table 3). We analyzed the genes encoding the digestive enzyme trehalase (*treh*), responsible for breaking down trehalose into two glucose molecules, and the enzyme sucrase-isomaltase (*SI*), which breaks down sucrose into one molecule of glucose and one of fructose in the small intestine. We also examined genes encoding transporters involved in the absorption of these sugars from the intestinal lumen and into the blood, including the sodium/glucose cotransporter (SLC5A1/SGLT1), the solute carrier family 2 member 2 (SLC2A2/GLUT2), and the solute carrier family 2 member 5 (SLC2A5/GLUT5). Furthermore, glucose transporters are known to play crucial roles sequestering circulating blood glucose into cells to meet tissue-specific energy demands ((Navale & Paranjape, 2016; Supplemental Table 3). These included SLC2A1/GLUT1, present in the plasma membrane of most cells and enriched in astroyctes, SLC2A2, enriched in the liver, hypothalamus, and pancreatic beta cells, SLC2A3, predominantly found in neurons, SLC2A4/GLUT4, expressed in insulin-sensitive tissues such as cardiac muscle, skeletal muscle, and fat, and SLC2A5, enriched in microglia, liver, kidney, and testis.

Using aBSREL (adaptive branch-site random effects likelihood; Smith et al., 2015) with HyPhy (Pond et al., 2005; 2020), we performed unbiased branch-site tests to identify episodic positive selection on orthologous gene sequences (Supplemental Table 4). Along the ancestral branch of the vespertilionid family, particularly in the *Eptesicus* branch (Fig.2, Branch A), we detected signatures of selection in the trehalase gene (*Treh*). Surprisingly, the digestive enzyme sucrase-isomaltase gene (*SI)* and the transporter gene *Slc2a5* showed signs of selection in the vespertilionid lineage *Myotis*, potentially explaining their enhanced ability to assimilate sucrose compared to other insect-eaters (Fig. 1A). In the vampire bats (Fig. 2, Branch B), the ancestral branch leading to plant-eating (Fig. 2 Branch C), and the ancestral branch leading to nectar-eating (Fig. 2, node E), we found positive selection in the neuron-enriched *Slc2a3* gene. This suggests that neurons of vampire bats and nectar bats favor glucose uptake to meet the metabolic demands related to neuronal activity, probably associated with their unique locomotor activity (Ripperger & Carter, 2021; C. C. Voigt & Winter, 1999), foraging behavior (Winter & Stich, 2005; Ross & Holderied, 2013; Muchhala & Serrano, 2015; Ripperger & Carter, 2021), and sensitivity to starvation (McNab, 1973; Freitas et al., 2013; Amaral et al., 2019). Adding to this, we found positive selection in the gene *Slc2a1* in the nectar bat *Anoura caudifer*, which is enriched in brain astrocytes responsible for maintaining synaptic function.

In the ancestral branch leading to species with fruit diets, we observed no significant molecular adaptions, similar to a recent study on ancestral molecular evolution in Neotropical bats (Potter et al., 2021). However, we did identify a molecular adaptation related to glucose and fructose absorption in the genus *Sturnira* (Fig. 2, Branch D). We detected positive selection for the gene *Slc2a5*, which distinctively matches *in vivo* blood glucose levels observed in *Sturnira* after sucrose ingestion (368 mg/dL), a pattern not observed in other fruit bats like *Artibeus* or *Dermanura* (Figure 1A). *Musonycteris harrisonii* exhibited adaptations in *SI* and *Slc2a2*, *A. caudifer* showed adaptations in *SI*, and the ancestral branch leading to the genus *Leptonycteris* displayed adaptations in *Slc2a2*. In nectar bats (Figure 1A), we observed an increase in blood glucose levels 10 minutes after consuming sucrose, indicating the activity of SI and the likely absorption of glucose through SLC2A2. Similarly, in the nectar-feeding omnivore *Phyllostomus* (Figure 2, branch C), we found positive selection in *SI*. However, during the one-hour experiment, they did not assimilate significant amounts of glucose from digested sucrose (Figure 1A). This suggests that the adaptations in *SI* may facilitate dietary expansion to omnivory in *Phyllostomus*, allowing them to respond to seasonal changes in food availability, which is in line with the fact that ingesting high-sugar sources, like nectar, is expected to increase sugar metabolism proteins

(Kishi et al., 1999; Cui et al., 2003), particularly *SI* expression (Yasutake et al., 1995). Detailed results of the aBSREL analysis are provided in Supplemental Table 6 & 7.

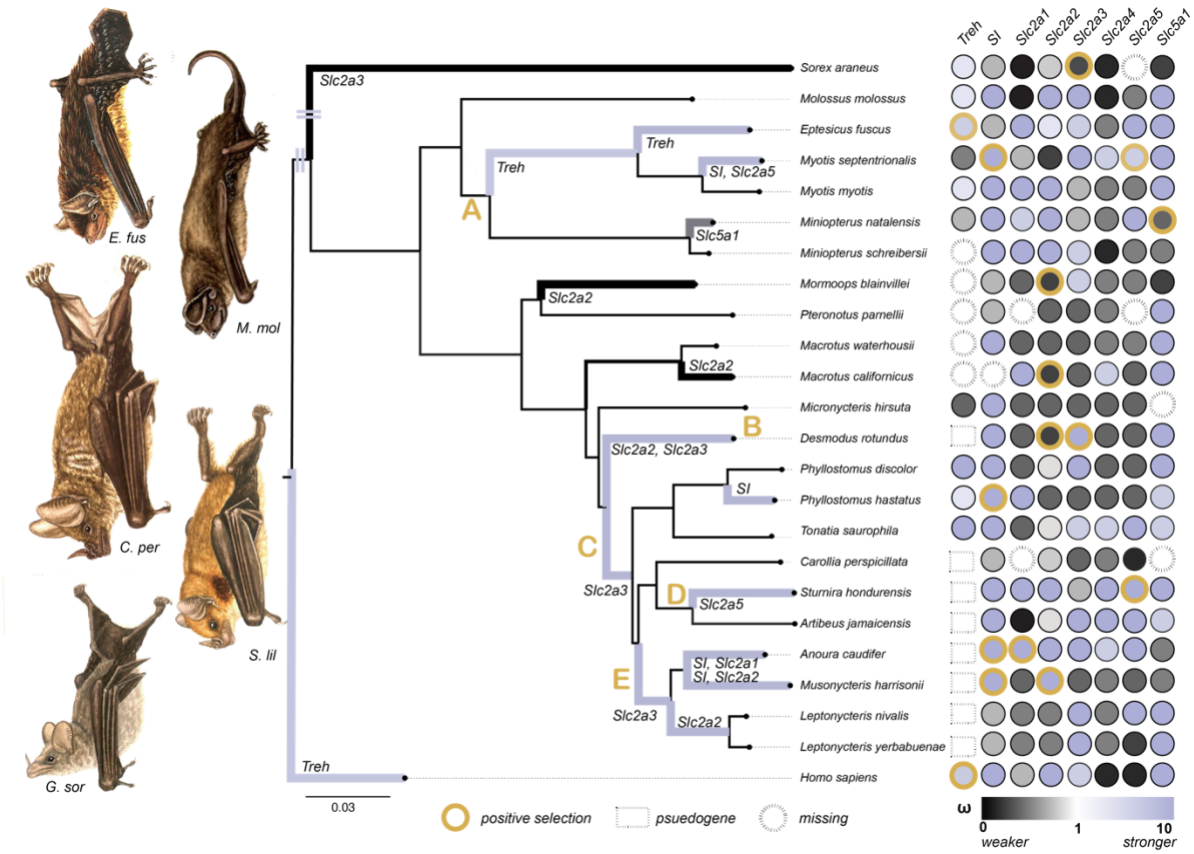

Fig. 2. Positive selection tests for candidate genes. Bat phylogeny is based on whole genome alignment, shown here with branch length related to substitution rate, except where a double line is marked. Outgroup species are human and shrew. A) Insect-feeding vespertilionid bat branch, B) blood-feeding, C) ancestral branch towards omnivores, D) fruit-eating, E) nectarivore ancestral branch. Each selection test per gene is summarized as a colored circle along each species branch from left to right as Trehalase (*Treh*), Sucrase-Isomaltase (*SI*), glucose transporter 1 (*Slc2a1*), glucose transporter 2 (*Slc2a2*), glucose transporter 3 (*Slc2a3*), glucose transporter 4 (*Slc2a4*), glucose transporter 5 (*Slc2a5*), and sodium/glucose cotransporter 1 (*Slc5a1*). Positive selection is indicated by color coding, where purple shading represents an omega value greater than 1, black shading represents an omega score less than 1, and significant positive selection ($p < 0.01$) is denoted by a circled gold marker. A summary of the significant results (<0.01) of the positive selection tests after Bonferroni correction are highlighted on the tree with a thicker line and with the gene(s) noted along the branch. Dotted squares are the evolutionary pseudogenized *Treh* within Phyllostomidae (Jiao et al., 2019) and dotted circles are genes missing in the genome due to inadequate sequencing depth. Bats drawn by Fiona Reid are *E. fus*: *Eptesicus fuscus*, insectivorous; *M. mol: Molossus molossus*, insectivorous*; C. per*: *Carollia perspicillata*, omnivorous; *S. lil*: *Sturnira lilium*, frugivorous; *G. sor*: *Glossophaga soricina*, nectar-eating bat.

Intestine anatomy

We next investigated key anatomical features of the small intestine, focusing on the duodenum, where the majority of glucose absorption occurs (Riesenfeld et al., 1980; Wright et al., 2018). In comparison to humans, bats lack circular folds in their small intestine (Silva et al., 2020), a finding that was

confirmed in our analysis. However, we observed striking differences in the intestinal length among bat species (Fig. 3), which were consistent with drawings by Park & Hall (1951). By comparing bats with different diets, we found a correlation between the duodenum length and the proportion of sugar in their diet. Bats with sugar-rich diets exhibited longer duodenum, suggesting anatomical adaptations to deal with increased sugars and plant material as they shifted from insectivory to frugivory/nectarivory.

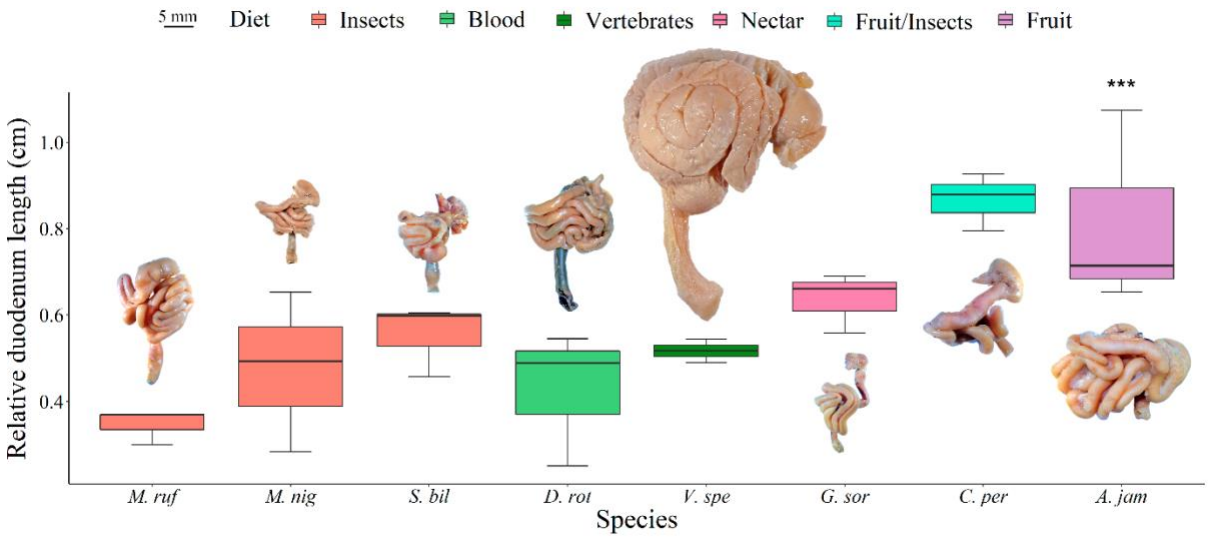

Fig. 3. Relative length of duodenum associated with gastrointestinal tract morphology from eight bat species with different diets. Duodeum length relative to torso length in each species (shoulders to rump). *S. bil*: *Saccopteryx bilineata*, insectivorous; *M. nig: Myotis nigricans*, insectivorous*; M. ruf*: *Molossus rufus*, insectivorous; *D. rot: Desmodus rotundus*, hematophagous; *V. spe*: carnivorous; *C. per*: *Carollia perspicillata*, omnivorous; *A. jam*: *Artibeus jamaicensis*, frugivorous; *G. sor*: *Glossophaga soricina*, nectar-eating bat. Three individuals per species reported, except *V. spe* with two individuals. Species with fruit and nectar diets tend to have longer duodenum than the blood, meat and insect-eating species.

The intestine plays a crucial role in nutrient absorption, particularly through specialized structures called villi that project into the gut lumen (Hilton, 1902; Walton et al., 2018). These villi consist of specialized epithelial cells (enterocytes) and goblet cells (Strobel et al., 2015), and in bats, they exhibit diverse shapes (Figure 4). Among the eight bat species examined, we observed common finger-like villi (Fig. 4D #1 & #2), previously described pyramidal villi (Figure 4D #4), and zigzag villi (Figure 4D #6) (Scillitani et al., 2007; Gadelha-Alves et al., 2008; Silva et al., 2020). Additionally, we found villi shapes (Figure 4D #3 & #5) that, to our knowledge, have not been reported before. In insectivorous bats, finger-like villi were primarily observed, some of which had simple entrances along the border (Fig. 4D black tringles). *Glossophaga* exhibited entrances and sometimes an additional "gap" in the middle of the villi body (Fig. 4D #3 blue triangle). Pyramidal-shaped villi (Fig. 4D #4) were found in *Carollia*, *Artibeus* and some *Myotis* individuals, while zig-zag villi (Fig. 4D #6) were mainly found in *Artibeus*, *Carollia*, with rare occurances in *Myotis*. *Glossophaga* also displayed pyramidal and zig-zag villi but with more pronounced entrances along the entire length of the villi. We identified a novel villi type (Fig, 4D #5), that we referred to as "ruffled", in *Carollia* and *Myotis*, characterized by multiple crests and troughs along its perimeter. The diverse villi morphologies observed suggest functional adaptations aimed at increasing the absorptive area in their duodenum.

We quantified the villus perimeter exposed to the lumen in the duodenum of species with different food preferences to asses its association with nutrient absorption. After adjusting for body size, we found a greater exposed surface area of villi in the duodenum for bats with sugar-rich diets (*Artibeus*,

Glossophaga, and *Carollia*), compared to insectivorous and vampire bats (Fig. 4A). The variation in duodenum villi exposure, combined with the *in vivo* physiology data, suggests that the increased absorptive area in the duodenum of bats with sugar-rich diets may contribute to enhanced glucose absorption (Fig. 1A). A similar pattern has been observed in the proximal intestine of the distantly related frugivorous megabat *Epomophorus wahlbergi* (Makanya et al., 1997).

Using Transmission Electron Microscopy (TEM), we visualized the enterocytes and their microvilli, which contribute to a 20-fold increase in the absorptive surface area (Helander & Fändriks, 2014; Price et al., 2015). We measured individual enterocytes, defined as the the distance between tight junctions, and quantified the number of microvilli per enterocyte. Our subcellular analysis revealed a higher number of enterocytes (Fig. 4B) and microvilli (Fig. 4C) in the duodenum of bats with rich-sugar diets, specially *Glossophaga* and *Artibeus* (maximum *in vivo* glucose levels of 600 mg/dL), compared to the insect and vampire bats, but specially compared to *Molossus* (maximum *in vivo* glucose levels of 174 mg/dL). This microvilli pattern observed in Neotropical bats is convergent with findings in old-world bats, where insect-eaters have smaller and fewer microvilli, while fruit bats have longer and more abundant microvilli (Makanya et al., 1997; 2005). The increased number of enterocytes and microvilli suggests enhanced paracellular absorption between intestinal cells (Caviedes-Vidal et al., 2008; Brun et al., 2014; Fasulo, 2014) and provides greater space for glucose transporters and digestive enzymes along the brush border (Price et al., 2015). These results indicate that bats with different diets have varying intestinal absorption capabilities. For example, in nectar and fruit-eating bats, the numerous microvilli could increase the density of SI and apical transporters (SLC5A1, SLC2A2, and SLC2A5), thereby promoting glucose absorption and elevated blood glucose levels (Fig. 1).

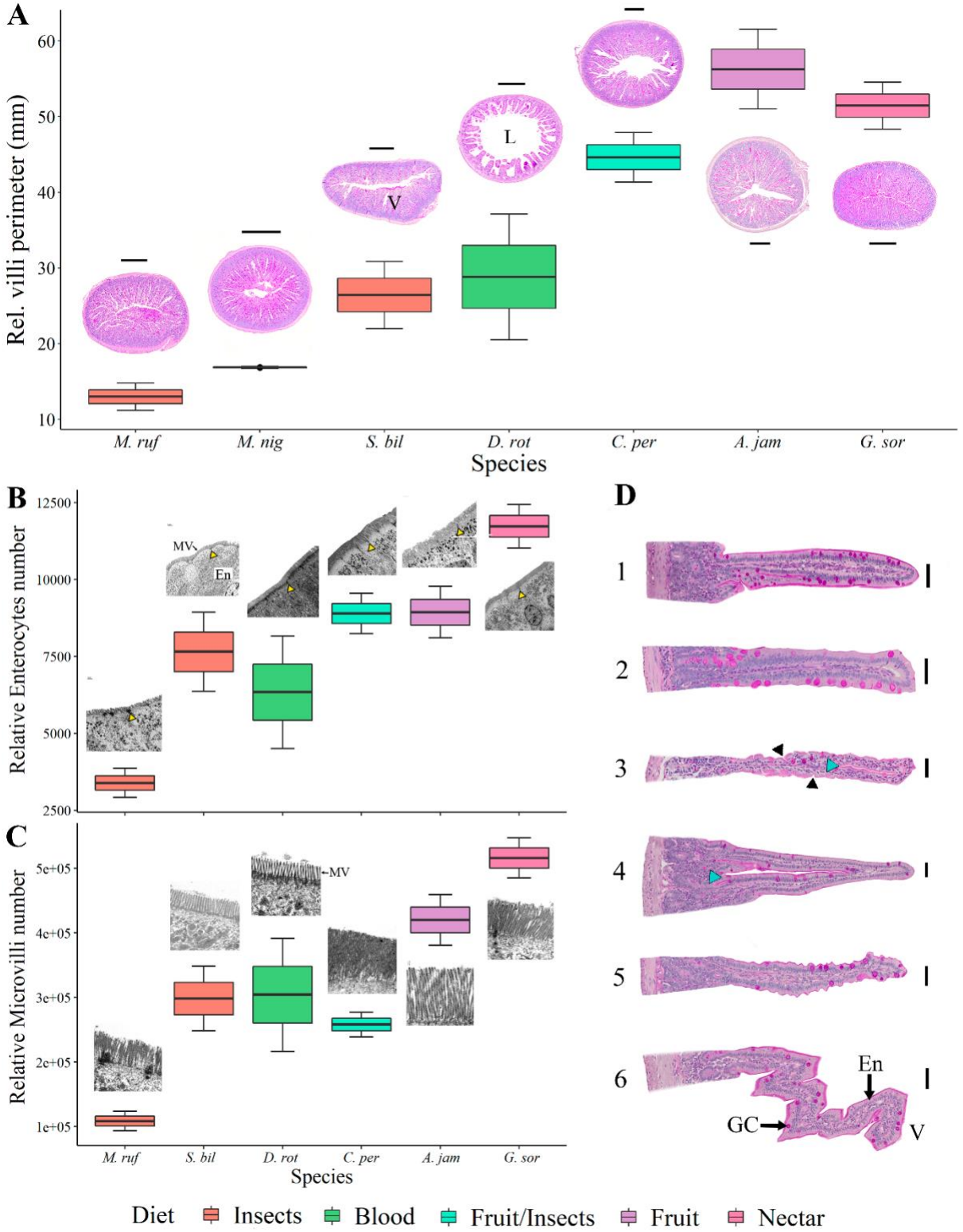

Figure 4: Histology of duodenum of bats with different diets. A. Relative villi perimeter across the duodenum related to cross-sections for each species; B. Relative number of enterocytes along the duodenum related to TEM of the enterocytes and microvilli; C. Relative number of microvilli along the duodenum related to TEM of microvilli. D. Different types of villi in bats, 1-2) finger-like villi, 3) finger-like villi with entrances (black triangle) and gap (blue triangle), 4) arch-like villi, 5) New villi "ruffled"; 6) zig-zag villi; (1, 4, 5 extracted from *C. per*; 2 from *S. bil*, 3 from *G. sor*, 6 from *A. jam*). Species *M. ruf*: *Molossus rufus*, *S. bil*: *Saccopteryx bilineata*,, *D. rot: Desmodus rotundus*, *C. per*:

Carollia perspicillata, *A. jam*: *Artibeus jamaicensis*, *G. sor*: *Glossophaga soricina*. A and D. Periodic acid-Schiff-staining. Scale bars: A. 250 µm, D. #1-3, 5: 20 µm, #4, 6: 25 µm. Yellow triangles pointing at tight junctions between enterocytes (En), MV: microvilli. V: villi, L: lumen, GC: Goblet cells. Measurements reported from one individual per species for the histology section and one individual per species for the TEM section.

Molecular mechanism of glucose absorption by transporters

Next, we investigated the molecular activity underlying glucose transcellular absorption and its impact on plasma glucose levels. We examined the *in vivo* glucose transfer from the gut lumen into the enterocyte through the key components of molecular glucose transcellular absorption: Na^+-dependent glucose co-transporter, SGLT1 (*Slc5a1*), the apical solute carrier family member 2 glucose transporter, GLUT2 (*Slc2a2*), and GLUT5 (*Slc2a5*) (Fig. 5a-c). To do this, we employed multiplexed, single-molecule HCR™ RNA-fluorescent in situ hybridization (RNA-FISH) on fasted bats to bats that were fed a single dose of glucose (5.4g/kg body weight) with a 20% glucose solution (~134mM of luminal glucose). In response to dietary glucose, the insectivorous bat, *Pteronotus parnellii*, displayed a log2 fold change of 1.9 in *Sglt1* expression and a log2 fold change of 1.1 in *Slc2a2* expression (Fig. 5d, 5e), accompanied by a rise of 184 mg/dl in their blood glucose levels (Sup Fig. 2). The omnivore *Carollia perspicillata*, exhibited an increase of 446 mg/dl in blood glucose levels (Sup Fig. 2), along a log2 fold change of 2.5 in *Sglt1* expression and 0.73 in *Slc2a2* expression. The nectar specialist, *Glossophaga soricina*, showed the highest blood glucose change of 617 mg/dl (Sup Fig. 2). Like *C. perspicillata*, the log2 fold change in *Sglt1* expression was 2.6. However, unlike in any mammal previously documented, the log2 fold change in *Slc2a2* expression was negligible at -0.1 (Sup. Fig. 2). Interestingly, the upregulation of *Slc2a2* expression during fasting and after feeding we observed in nectar bats, relative to other bats, has been also reported in the Ruby-throated Hummingbird, providing a notable example of convergent evolution (Ali et al., 2020).

Given the high glucose concentration present in their liquid nectar diets and their extremely high postprandial glucose levels, we attribute the distinctive expression pattern of *Slc2a2* as an adaptation specific to nectarivorous bats. The permanent presence of apical SLC2A2 might result from defective insulin action, as insulin typically triggers the internalization of SLC2A2 to slow down sugar uptake and prevent high blood glucose levels after a sugar meal (Tobin et al., 2008). This is in line with the fact that nectar feeding bats need to absorb high quantities of glucose to fuel their energetic requirements (Suarez & Welch, 2017; Voigt & Speakman, 2007) and the hypothesis about additional mechanisms, complementary to insulin, to regulate glucose homeostasis (Kelm et al., 2011; Peng et al., 2017). The magnitude of postprandial hyperglycemia observed in nectars bats provides strong evidence that the adaptation towards nectar-feeding has primed the duodenum for immediate and enhanced dietary sugar absorption, ensuring an adequate supply glucose to tissues. This adaptation is further supported by the permanent apical expression of *Slc2a2* associated with obesity and diabetes, conditions characterized by high blood glucose levels, insulin resistance, and an increase in villous surface area (Marks et al., 2003; Ait-Omar et al., 2011; Gromova et al., 2021). Therefore, the long-term dietary adaptations modify the fundamental regulation of glucose absorption at the level of the enterocyte via transporter trafficking in addition to the well-known paracellular absorption mechanism.

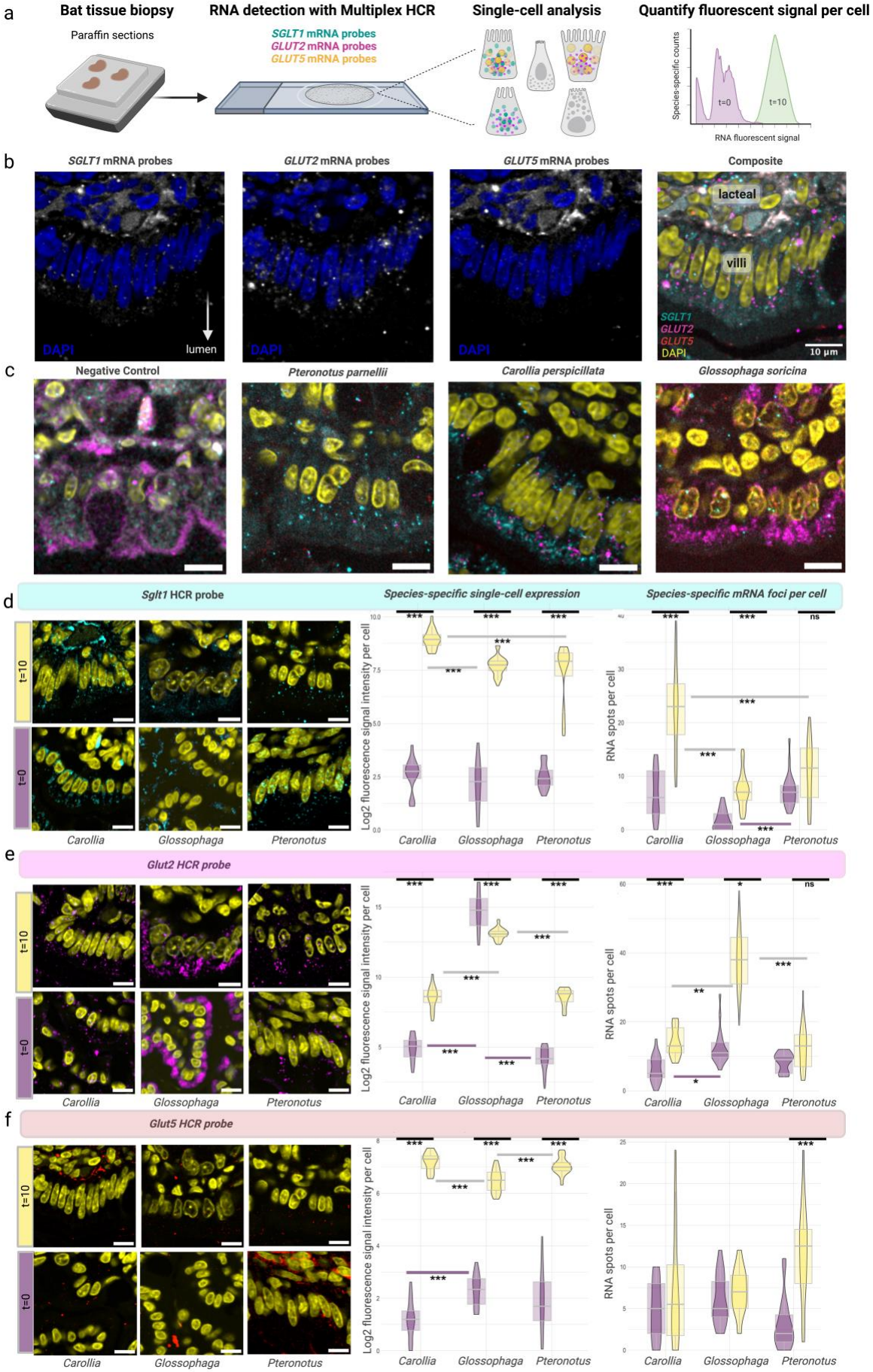
a
Bat tissue biopsy
Paraffin sections
RNA detection with Multiplex HCR
SGLT1 mRNA probes
GLUT2 mRNA probes
GLUT5 mRNA probes
Single-cell analysis
Quantify fluorescent signal per cell
Species-specific counts
t=0
t=10
RNA fluorescent signal
b
SGLT1 mRNA probes
GLUT2 mRNA probes
GLUT5 mRNA probes
Composite
DAPI
lumen
lacteal
villi
SGLT1
GLUT2
GLUT5
DAPI
10 µm
c
Negative Control
Pteronotus parnellii
Carollia perspicillata
Glossophaga soricina
d
Sglt1 HCR probe
Species-specific single-cell expression
Species-specific mRNA foci per cell
t=10
t=0
Log2 fluorescence signal intensity per cell
RNA spots per cell
Carollia
Glossophaga
Pteronotus
e
Glut2 HCR probe
f
Glut5 HCR probe

Figure 5: HCR RNA-FISH in the duodenum of bats from different diets. A) We performed HCR RNA-FISH with probe sets targeting *Sglt1*, *Slc2a2* (*Glut2*) and *Slc2a5* (*Glut5*) on fixed paraffin embedded bat tissue, and quantified log2 RNA fluorescent signal per enterocyte and the number of RNA foci per enterocyte. RNA expression was compared in fasted bats (n=2 per species) and bats fed a single dose (5.4mg/kg body weight) of glucose (n=2 per species). B) Example images of the duodenum with each probe set isolated from the composite image. C) Example images of each species and the negative control (no probes). D-F) Results of the image analysis taken from 20 cells at fasted (t=0) and fed (t=10). We found that for each probe set the fed bats had significantly different fluorescent intensities compared to fasted bats. D) *Sglt1* fluorescence signal (cyan) in response to glucose is highest in *Carollia* and similar between *Pteronotus* and *Glossophaga*. E) *Glut2* fluorescence signal (magenta) is high in *Glossophaga* at fasting. In response to glucose, *Pteronotus* and *Carollia* have similar signal intensity and spots. F) Fluorescence signal from Glut5 (red) is lowest in *Glossophaga* in response to glucose. The scale bar is 10 microns. DAPI (yellow) labels the cell nuclei. P-values: >2e-13 (***), >0.001 (**), >0.01 (*) after adjusting for multiple pairwise comparisons using Games-Howell test.

Conclusion

Our integrative approach reveals that the differences in sugar assimilation among Neotropical bats directly correlate with their dietary evolution and provides valuable insights about metabolic adaptations. Enzymes, glucose transporters, and absorptive gut traits have undergone adaptive selection, enabling the transition from an insect-eater ancestor to species with diverse diets. Through a multidisciplinary approach, encompassing *in vivo* physiology measurements, genomics, gut anatomy, and single molecule analysis, we have unraveled the intricately linked mechanisms underlying sugar assimilation in these remarkable mammals. These findings have broader implications for our understanding of blood glucose regulation and provide a foundation for future investigations into the interplay between genotype, phenotype, and ecological factors. Further exploration of the molecular and physiological adaptations in bats will undoubtedly enrich our understanding of the evolutionary dynamics that shape the diversity of life on our planet.

Methods

Field work

The fieldwork was made under the permit of the National Authority of Environmental Licenses and the Ministry of Environment and Sustainable Development of Colombia, Resolution 1070, August 28th, 2015. Bats were captured between June 2019 and December 2020 in 11 localities of the dry tropical forest ecosystem in the department of Valle del Cauca, Colombia, some within the Dry Tropical Project from the Institute for Research and Preservation of the Cultural and Natural Heritage of Valle del Cauca (INCIVA). To catch species with different food preferences (frugivores, insectivores, nectarivores, omnivores and hematophages), we opened mist nets between 18:00 and 24:00 h. In some instances, bats were manually captured in their refuge. Each individual was taxonomically identified, and their weight, age, sex, reproductive status and diet type was recorded. The diet of the species was classified into trophic categories according to their food preference and morphological adaptations for the consumption of the food resource (Park & Hall, 1951; Freeman, 1998; Rojas et al., 2011; Santana et al., 2011). In this way, the species of the genera *Artibeus*, *Dermanura*, *Uroderma* and *Sturnira* are considered frugivores, *Carollia* and *Phyllostomus* as omnivores, *Glossophaga* and *Choeroniscus* are

considered nectarivores, *Desmodus* hematophagous, *Vampyrum* as carnivore and *Saccopteryx*, *Peropteryx*, *Myotis* and *Molossus* as insectivorous. Here we include data for 79 individuals with preference for fruits, 55 omnivorous bats, 18 with preference for nectar, 15 for insects, 14 for blood and 1 carnivorous bat (Supplementary information, Table 1). Juvenile individuals and pregnant or lactating females were excluded from the study due to high energy requirements and significant physiological changes during these stages, compared to non-pregnant or non-lactating adult individuals (Kurta et al., 1989; C. Voigt, 2003).

1.2 *Oral glucose tolerance tests*

After identification, bats were fed a 20% sugar solution and subsequently subjected to a period of fasting for at least ten hours. After fasting, a bat was fed a bolus of sugar (5.4g/kg of body weight) as previously established by Kelm et al. (2011). Individual bats were only fed one type of sugar (Glucose, Sucrose, or Trehalose). To determine blood glucose levels, a drop of blood was drawn from the forearm with a 30G lancet before the sugar bolus and 10, 30, and 60 minutes post-feeding. The blood was immediately measured using a GlucoQuick G30a glucometer (Diabetrics®) with a range of 20-600 mg/dL. The bats individually remained in cloth bags between readings. Finally, the bats were tagged, fed, and released. In total, blood glucose was measured for 194 individuals from 27 species and four families: Phyllostomidae, Emballonuridae, Vespertilionidae and Molossidae.

1.2.1 *General patterns of sugar assimilation curves*

We proposed general curves (Figure 1B) for the description of the temporal pattern of assimilation of different sugars in Neotropical bats based on a 1 hour glucose tolerance test. The glucose curves were classified according to the speed of sugar assimilation to facilitate the understanding of the behavior of the curves. The *"Fast"* assimilation curve shows a peak of blood glucose levels only after 10 min of sugar ingestion, followed by a decrease of blood glucose levels. The *"Medium"* assimilation curve shows a peak of blood glucose levels 30 min after sugar ingestion followed by a decrease in blood glucose levels. The *"Slow"* assimilation curve shows a continuous increase in blood glucose levels until the final timepoint, with the maximum levels 60 min after sugar ingestion. Finally, the *"Limited"* assimilation curve shows blood glucose levels with little variation throughout the different time points of the test.

1.3 *Statistical analysis*

Blood glucose levels of all bats measured were grouped by species and plotted in R (Figure 1). Afterwards, we evaluated the phylogenetic signal for the assimilation of the various carbohydrates by the Pagel λ index (Pagel, 1999) at the first (10 min) and last (60 min) blood sugar measurement. We termed the difference between these two values as the assimilation pattern estimate (APEs). APE was evaluated by a Phylogenetic Generalized Least Squares (PGLS) analysis with Brownian Motion employing ML (Symonds & Blomberg, 2014). The models were compared using the Akaike information criterion (AIC; Akaike, 1974). The analysis was made using a phylogeny extracted from Vertlife (Upham et al., 2019) using ape (Paradis & Schliep, 2018), phytools (Revell, 2012) and Geiger (Pennell et al., 2014) packages in the R 3.6.1 programming language (R Core Team, 2019).

2.1 *Morphology and histology of the GI tract*

We extracted the GI tract from individuals preserved in 70% ethanol from species obtained in previous studies on bats (Camacho et al., 2020) obtained under the Wildlife Section, Forestry Division, Ministry

of Agriculture, Land and Marine Resources (Republic of Trinidad and Tobago) permit number 1737 (2014). The species incorporated in this section were *Glossophaga soricina*, *Artibeus jamaicensis*, *Carollia perspicillata*, *Molossus rufus* and *Saccopteryx bilineata*. Additionally, we included two species obtained from the KU Biodiversity Institute and Natural History Museum: *Myotis nigricans* (KU 134846) and *Desmodus rotundus* (KU 100374), and one species obtained from the American Museum of Natural History: *Vampyrum spectrum* (M-267445, 272936). Finally we added more individuals to the analysis from the AMNH (*A. Jamaicensis* 7473; *C. perspicillata* 7458, 175795; M. rufus 178675, 178672; *S. bilineata* 184693, 149982; *M. nigricans* 175725, 175724; *D. rotundus* 175406, 239943). We measured the length of the duodenum through imaging the unfolded-stretched intestine of each species with a Canon EOS Rebel E7i. Then we determined the length through the Fiji platform – Image J 1.53f51 (Schindelin et al., 2012), and we compared relative intestine length as the gut length divided by torso length (shoulders to rump length). We used this measure to control by body size due to our focus on the intestine and where it is located, without adding measures related to the length of the rostrum or the tail, which can vary across bat species.

The main segment of the small intestine responsible for sugar absorption, the duodenum, was further analyzed with histology. The duodenum is the first section of the intestine from the end of the stomach-pylorus to the duodenojejunal flexure (Ishida et al., 2018). The duodenum was recognized by its greater diameter compared to the jejunum, the next intestine section after the duodenum. Histologically, the proximal duodenum contains brunner glands (Bhide, 1978).

For histology comparisons we cut 0.5-1 cm sections of the duodenum. The gut tissues were embedded in paraffin, serially cross-sectioned to 10 µm, and stained with periodic acid–Schiff (PAS). All tissues were imaged using an Olympus slide scanner equipped with a 20X objective exported as a TIFF. Two sections with good morphology per individual were chosen for study. We measured the area of villi and lumen (VLA) in each cross section, and then we delimited 1/10 of VLA to measure the well-preserved villi perimeter (VPSA) in this sample area (SA). We also measured the lumen area (LA) so we could calculate the total villi perimeter along the cross section. Then we corrected the measurement for size difference among species by considering the cross-section perimeter (CSP) from the different species. Finally, we extrapolated the final value from villi exposed in the whole cross section corrected by size, to the relative duodenum (D) length (Eq. 1). (Measures summarized in Supplemental Figure 1).

Equation 1. Villi in Duodenum (Vduo) = (((VPSA*(VLA-LA))/SA)/CSP)* Relative length of D.

2.2 Transmission electron microscopy

To look closer at the enterocytes and microvilli, we used transmission electron microscopy (TEM). We sectioned 0.5-1.0 cm of duodenum from the above-mentioned species. The samples were rehydrated and fixed in 50 mM Sodium Cacodylate (pH 7.4) containing 2.5% Paraformaldehyde and 2% Glutaraldehyde. The tissue segments were then post-fixed with 2% OsO4 for 2 hours, washed, and stained with 1% aqueous Uranyl Acetate overnight. After dehydration with a gradient of Ethanol, the samples were infiltrated and embedded into Epon resin. Ultrathin (80 nm) sections were cut with a Leica UC7 Ultramicrotome, collected onto slot copper grids, and stained with 4% Uranyl Acetate in 70% Methanol and Sato's triple lead solution. Sections were imaged using a FEI transmission electron microscope at 80kV using the DigitalMicrograph® software.

To calculate the number of enterocytes in the duodenum we measured the enterocyte width of five different cells from each species and the average was extrapolated to the relative length of the duodenum by dividing the villi surface found in the duodenum by the enterocyte width average. In addition, for calculating the number of microvilli in the duodenum, we counted the number of microvilli in each of the five different enterocytes where we measure the width, and then we multiplied the average microvilli

value by the number of enterocytes. All the measurements were made with the Fiji platform – Image J 1.53f51 (Schindelin et al., 2012).

3.1 Genomics

Genome assemblies for 22 Chiroptera species, which includes representatives from each of the dietary groups, were downloaded from online sources (Supplemental Table 1). Transcriptomes and proteomes for 16 species were obtained from the National Center for Biotechnology Information (NCBI) and Ensembl databases (Supplemental Table 1). After filtering out genomic contigs less than 10kb we generated gene models using MAKER (v3.01.03) using the 16 transcriptomes and proteomes (plus SwissProt/Uniprot v2021_03) as "EST evidence" and "Protein Homology Evidence". RepeatMasker (open-4.0.7 with DB version 20170127) was used by MAKER to identify mammalian repeats. Links to the versions of all publicly available data (genome assemblies, transcriptomes, proteomes) used by MAKER can be accessed on SIMRbase (https://simrbase.stowers.org/bats_sugar_assimilation). Our SIMR bat models were assigned names derived from Uniprot (UniProt consortium, 2020) best hit with an evalue <= 1e-5. SIMR bat models are available for download and for browsing on SIMRbase (https://simrbase.stowers.org/bats/data). Genome browsers were built using Jbrowse (Buels et al., 2016) and SIMR buelsbase was built using Tripal (Spoor et al., 2019).

3.2 Ortholog Assignment and Candidate Gene Identification

To relate the blood glucose tolerance assay to evolution, we identified genes involved in sugar assimilation, specifically from the gut absorption into the bloodstream. A short list of eight genes (Table S3) were identified as having biased function and expression in the duodenum using mouse ENCODE (NCBI Bioproject PRJNA66167) and human HPA (NCBI Bioproject PRJEB4337). Orthologs were assigned to the SIMR bat models with standalone Orthologous Matrix (OMA) (version 2.4.2) using three species included in the OMA FASTA database (April 2021), *Homo sapiens* (HUMAN), *Pteropus vampyrus* (PTEVA), and *Myotis lucifugus* (MYOLU). A gene is considered an ortholog if it is found in the same OMA ortholog group (OG) as a HUMAN candidate gene with appropriate HGNC identifiers (Table S4).

3.3 Phylogenetic analysis of sugar related genes

Whole genome alignments of single-copy orthologs trimmed with trimAl v1.4.rev15 (Capella-Gutiérrez et al., 2009) from 22 SIMR bat models and two outgroups (Supp Table 1) were used to generate a phylogenomic tree (Dylus et al., 2022) using RaxML version 8.1.15 (PROTFAMMAUTO model). Our molecular phylogeny, which matches published species topologies (Rojas et al., 2016; Potter et al., 2021), includes a broad taxonomic sampling, incorporating Miniopteridae, Vespertilionidae, and Molossidae (Figure 2, Branch A; Miller-Butterworth et al., 2007; Lim, 2009). The resulting phylogeny was used for all exploratory selection tests of candidate genes along all branches (Table S3). The tested DNA sequences were from single-copy orthologs found using OMA (Table S4). For selection tests, we used the codon-based method measuring non-synonymous (dN) to synonymous nucleotide (dS) substitutions (the dN/dS metric, **ω**) with the tool HyPhy (www.hyphy.org). To identify branches under positive selection, aBSREL (adaptive branch-site random effects likelihood) was used (Smith *et al.* 2015). For detection of genetic sites under positive selection, MEME (mixed effects model of evolution) was used on all branches (Murrell et al., 2012).

3.4 HCR™ RNA-fluorescent in situ hybridization

The glucose tolerance tests (n=4; Supp Fig. 2) were performed on *Pteronotus parnellii* (insect bat), *Carollia perspicillata* (piper-insect bat), and *Glossophaga soricina* (nectar bat) in April 2022 with permission from the Republic of Trinidad and Tobago. To determine blood glucose levels, a drop of blood was drawn from the forearm with a 30G lancet before the sugar bolus and 10 minutes post-feeding. The blood was immediately measured using an AlphaTRAK 2.0 glucometer (Zoetis®) with a range of 20-750mg/dl calibrated for cats (health range 120-300mg/dl). Finally, the bats were euthanized (n=2 per species) and the tissue was dissected, fixed and stored in 4% paraformaldehyde.

Fluorescently labeled HCR hairpins targeting *Slc5a1* (*Sglt1)*, *Slc2a2* (*Glut2*), and *Slc2a5* (*Glut5*) in fasted and fed bats were purchased from Molecular Technologies and 3rd generation HCR RNA-FISH was performed on 10 µm paraffin sections of the duodenum. Slides were deparaffinized and microwave antigen retrieval was applied at 95°C for 15 min. Hydrophobic barrier was created using ImmEdge® Hydrophobic Barrier PAP Pen (Vector laboratories) around the sections on slide, and bleaching solution (3% H2O2, 5% formamide, 0.5X SSC) was applied for 30 min under strong LED light. Tissue sections were permeabilized with Proteinase K (20 ug/mL) for 12 min at room temperature, washed with PBS five times, incubated in hybridization buffer for 30 min at 37°C, then incubated in Hybridization buffer containing probes at 37°C for 16 hours. Tissue sections were washed 5 times with the wash buffer for 5 min each, then 2 times in the 5 X SSCT (5X SSC + 0.1% Tween 20). Fluorescently labeled HCR amplifiers were snap-cooled by heating at 95°C for 90 s and cooling to room temperature for 30 min under dark conditions and added to the amplification buffer. Tissue sections were incubated in the amplification buffer for 30 min at room temperature and incubated in amplification buffer containing amplifiers overnight at room temperature in humid chamber under the dark condition. Slides were washed 4 times in 5x SSCT for 5 min each, stained with DAPI (10ug/ml) in 5X SSCT for 30 min, then washed 2 times in 5X SSCT. Prolong gold (Invitrogen) was mounted and slides were stored at 4°C until imaging.

3.5 Image analysis

Images were taken on a Nikon Ti Exclipse with CSU-W1 spinning disk confocal microscope at 40x magnification. Fiji software was used to manually segment 5 cells per section and each cell (20 per treatment per species) was used for quantification of fluorescence signal using threshold-based segmentation and spot detection. Two sections with good morphology per individual were chosen for study.

4.1 Data depository

Detailed data about the genomics analysis can be found here: https://simrbase.stowers.org/.

Acknowledgements:

This work was possible thanks to academic groups, personal and scientific funding efforts. A portion of the fieldwork was carried out within the framework of the project "Contribución a la conservación del Bosque seco Tropical del Valle del Cauca" under the CVC permit No. 1122 of 2018, from the Institute for Research and Preservation of the Cultural and Natural Heritage of Valle del Cauca (INCIVA), whom we thank, along with the support of Jose Omar Ortíz, Ruth Rivera and Andrés Bernal, and the field assistance from Therios (Cali, Colombia), Cristian Calvache, Sergio Tabares, Alejandro Chito and Oscar Cuellar. We also thank Jose Alejandro Riascos for the bat illustration in the graphical

abstract. We also thank Darshan Narang and Richard Smith for their support in Trinidad. Thanks to Maria Eifler at the KU Biodiversity Institute and Natural History Museum, Nancy Simmons and Marisa Surovy from the AMNH for facilitating access and research of museum specimens. Funding for the project was provided by the Stowers Institute for Medical Research to N.R. and NSF Postdoctoral Research Fellowships in Biology #2109717 (2021-2022) to J.C. We thank the SIMR Histology core members Seth Malloy, Hannah Wilson, and Michael Frangello, Cindy Maddera from the Microscopy core and Xia Zhao for the help processing the EM sections. Finally, we thank the Rohner lab members for creating a stimulating scientific environment and for the support during the manuscript writing.

Author contributions:

A.B.R. and J.C. designed the study and figures. A.B.R performed the *in vivo* physiology experiments as an undergraduate thesis project (2019-2020) directed by O.E.M.G. A.B.R. and O.E.M.G. performed the statistical analyses for the *in vivo* physiology. J.C. and A.B.R. performed additional glucose tolerance tests and obtained tissue for molecular analyese in April 2022. A.B.R. and J.C. dissected the gastrointestinal tract of museum bats and performed morphological data interpretation. K.Y. performed the TEM experiments and imaging. A.B.R. made the gut anatomy measurements and comparisons. S.R. produced gene models across the assembled genomes, assigned orthologs, built webpages and genome browsers, and generated the phylogenomic tree. J.R. and J.C. performed selection tests. D.T. and Y.W. performed the HCR experiments and J.C. performed imaging and analysis. A.B.R., J.C., and N.R. co-wrote the manuscript.

References

Ait-Omar, A., Monteiro-Sepulveda, M., Poitou, C., Le Gall, M., Cotillard, A., Gilet, J., Garbin, K., Houllier, A., Château, D., Lacombe, A., Veyrie, N., Hugol, D., Tordjman, J., Magnan, C., Serradas, P., Clément, K., Leturque, A., & Brot-Laroche, E. (2011). GLUT2 Accumulation in Enterocyte Apical and Intracellular Membranes. *Diabetes*, *60*(10), 2598–2607. https://doi.org/10.2337/db10-1740

Akaike, H. (1974). A new look at the statistical model identification. *IEEE Transactions on Automatic Control*, *19*(6), 716–723. https://doi.org/10.1109/TAC.1974.1100705

Ali, R. S., Dick, M. F., Muhammad, S., Sarver, D., Hou, L., Wong, G. W., & Welch, K. C., Jr. (2020). Glucose transporter expression and regulation following a fast in the ruby-throated hummingbird, Archilochus colubris. *Journal of Experimental Biology*, *223*(20), jeb229989. https://doi.org/10.1242/jeb.229989

Amaral, T. S., Pinheiro, E. C., Freitas, M. B., & Aguiar, L. M. S. (2019). Low energy reserves are associated with fasting susceptibility in Neotropical nectar bats Glossophaga soricina. *Brazilian Journal of Biology*, *79*(2), 165–168. https://doi.org/10.1590/1519-6984.169674

Ayala-Berdon, J., Rodríguez-Peña, N., García Leal, C., Stoner, K. E., & Schondube, J. E. (2013). Sugar gustatory thresholds and sugar selection in two species of Neotropical nectar-eating bats. *Comparative Biochemistry and Physiology Part A: Molecular & Integrative Physiology*, *164*(2), 307–313. https://doi.org/10.1016/j.cbpa.2012.10.019

Baker, H. G., Baker, I., & Hodges, S. A. (1998). Sugar Composition of Nectars and Fruits Consumed by Birds and Bats in the Tropics and Subtropics1. *Biotropica*, *30*(4), 559–586. https://doi.org/10.1111/j.1744-7429.1998.tb00097.x

Bhide, S. A. (1978). Brunner's glands in some Indian Bats. *Current Science*, *47*(16), 571–573.

Brun, A., Price, E. R., Gontero-Fourcade, M. N., Fernandez-Marinone, G., Cruz-Neto, A. P., Karasov, W. H., & Caviedes-Vidal, E. (2014). High paracellular nutrient absorption in intact bats is associated with high paracellular permeability in perfused intestinal segments. *Journal of Experimental Biology*, *217*(18), 3311–3317. https://doi.org/10.1242/jeb.104927

Buels, R., Yao, E., Diesh, C. M., Hayes, R. D., Munoz-Torres, M., Helt, G., Goodstein, D. M., Elsik, C. G., Lewis, S. E., Stein, L., & Holmes, I. H. (2016). JBrowse: A dynamic web platform for genome visualization and analysis. *Genome Biology*, *17*(1), 66. https://doi.org/10.1186/s13059-016-0924-1

Camacho, J., Moon, R., Smith, S. K., Lin, J. D., Randolph, C., Rasweiler, J. J., Behringer, R. R., & Abzhanov, A. (2020). Differential cellular proliferation underlies heterochronic generation of cranial diversity in phyllostomid bats. *EvoDevo*, *11*, 11. https://doi.org/10.1186/s13227-020-00156-9

Capella-Gutiérrez, S., Silla-Martínez, J. M., & Gabaldón, T. (2009). trimAl: A tool for automated alignment trimming in large-scale phylogenetic analyses. *Bioinformatics*, *25*(15), 1972–1973. https://doi.org/10.1093/bioinformatics/btp348

Castro, D. L. J., Freitas, R. M. P., Silva, S. B., De Melo, F. C. S. A., Sarandy, M. M., Ospina, E. G., Sartori, S. R., Gonçalves, R. V., & Freitas, M. B. (2021). Insulin and glucose regulation at rest and during flight in a Neotropical nectar-feeding bat. *Mammalian Biology*, *101*(6), 987–996. https://doi.org/10.1007/s42991-021-00146-x

Caviedes-Vidal, E., Karasov, W. H., Chediack, J. G., Fasulo, V., Cruz-Neto, A. P., & Otani, L. (2008). Paracellular Absorption: A Bat Breaks the Mammal Paradigm. *PLOS ONE*, *3*(1), e1425. https://doi.org/10.1371/journal.pone.0001425

Cui, X.-L., Jiang, L., & Ferraris, R. P. (2003). Regulation of rat intestinal GLUT2 mRNA abundance by luminal and systemic factors. *Biochimica et Biophysica Acta (BBA) - Biomembranes*, *1612*(2), 178–185. https://doi.org/10.1016/S0005-2736(03)00129-9

Dylus, D., Nevers, Y., Altenhoff, A., Gürtler, A., Dessimoz, C., & Glover, N. (2022). How to build phylogenetic species trees with OMA. *F1000Research*, *9*, 511. https://doi.org/10.12688/f1000research.23790.2

Fasulo, S. V. (2014). Absorción Intestinal En Mamíferos. Evaluación Comparativa De La Ruta Paracelular En Mamíferos Terrestres Y Voladores. *Mastozoología Neotropical*, *21*(1), 180–181.

Freeman, P. W. (1998). Form, Function, and Evolution in Skulls and Teeth of Bats. In *Bats teeth and skulls*. Papers in natural resources.

Freitas, M. B., Queiroz, J. F., Dias Gomes, C. I., Collares-Buzato, C. B., Barbosa, H. C., Boschero, A. C., Gonçalves, C. A., & Pinheiro, E. C. (2013). Reduced insulin secretion and glucose intolerance are involved in the fasting susceptibility of common vampire bats. *General and Comparative Endocrinology*, *183*, 1–6. https://doi.org/10.1016/j.ygcen.2012.11.023

Gadelha-Alves, R., Rozensztranch, A. M. D. S., & Rocha- Barbosa, O. (2008). Comparative Intestinal Histomorphology of Five Species of Phyllostomid Bats (Phyllostomidae, Microchiroptera): Ecomorphological Relations with Alimentary Habits. *International Journal of Morphology*, *26*(3). https://doi.org/10.4067/S0717-95022008000300014

Gromova, L. V., Fetissov, S. O., & Gruzdkov, A. A. (2021). Mechanisms of Glucose Absorption in the Small Intestine in Health and Metabolic Diseases and Their Role in Appetite Regulation. *Nutrients*, *13*(7), 2474. https://doi.org/10.3390/nu13072474

Helander, H. F., & Fändriks, L. (2014). Surface area of the digestive tract – revisited. *Scandinavian Journal of Gastroenterology*, *49*(6), 681–689. https://doi.org/10.3109/00365521.2014.898326

Hilton, W. A. (1902). The morphology and development of intestinal folds and Villi in vertibrates. *American Journal of Anatomy*, *1*(4), 459–505. https://doi.org/10.1002/aja.1000010406

Ingala, M. R., Simmons, N. B., Dunbar, M., Wultsch, C., Krampis, K., & Perkins, S. L. (2021). You are more than what you eat: Potentially adaptive enrichment of microbiome functions across bat dietary niches. *Animal Microbiome*, *3*(1), 82. https://doi.org/10.1186/s42523-021-00139-8

Ishida, M., Sakata, N., Ise, I., Ono, T., Shimura, M., Ishii, K., Murakami, M., Takadate, T., Aoki, T., Kudo, K., Ohnuma, S., Fukase, K., Ohtsuka, H., Mizuma, M., Hayashi, H., Nakagawa, K., Morikawa, T., Motoi, F., Naitoh, T., & Unno, M. (2018). The comparative anatomy of the folds, fossae, and adhesions around the duodenojejunal flexure in mammals. *Folia Morphologica*, *77*(2), 286–292. https://doi.org/10.5603/FM.a2017.0089

Jiao, H., Zhang, L., Xie, H.-W., Simmons, N. B., Liu, H., & Zhao, H. (2019). Trehalase Gene as a Molecular Signature of Dietary Diversification in Mammals. *Molecular Biology and Evolution*, *36*(10), 2171–2183. https://doi.org/10.1093/molbev/msz127

Kelm, D. H., Simon, R., Kuhlow, D., Voigt, C. C., & Ristow, M. (2011). High activity enables life on a high-sugar diet: Blood glucose regulation in nectar-feeding bats. *Proceedings of the Royal Society B: Biological Sciences*, *278*(1724), 3490–3496. https://doi.org/10.1098/rspb.2011.0465

Kishi, K., Tanaka, T., Igawa, M., Takase, S., & Goda, T. (1999). Sucrase-Isomaltase and Hexose Transporter Gene Expressions Are Coordinately Enhanced by Dietary Fructose in Rat Jejunum. *The Journal of Nutrition*, *129*(5), 953–956. https://doi.org/10.1093/jn/129.5.953

Kurta, A., Bell, G. P., Nagy, K. A., & Kunz, T. H. (1989). Energetics of Pregnancy and Lactation in Freeranging Little Brown Bats (Myotis lucifugus). *Physiological Zoology*, *62*(3), 804–818. https://doi.org/10.1086/physzool.62.3.30157928

Lim, B. (2009). Review of the Origins and Biogeography of Bats in South America. *Chiroptera Neotrop*, *15*.

Makanya, A., John, M., Mayhew, T., Tschanz, S., & Burri, P. (1997). A Stereological Comparison of Villous and Microvillous Surfaces in Small Intestines of Frugivorous and Entomophagous Bats: Species, Inter-Individual and Craniocaudal Differences. *The Journal of Experimental Biology*, *200*, 2415–2423. https://doi.org/10.1242/jeb.200.18.2415

Makanya, A. N., Self, T. J., Warui, C. N., & Mwangi, D. K. (2005). GUT MORPHOLOGY AND MORPHOMETRY IN THE EPAULETTED WAHLBERGS FRUIT BAT (EPOMOPHORUS WAHLBERGI, SUNDEVALL, 1846). *Acta Biologica Hungarica*, *52*(1), 75–89. https://doi.org/10.1556/abiol.52.2001.1.8

Marks, J., Carvou, N. J. C., Debnam, E. S., Srai, S. K., & Unwin, R. J. (2003). Diabetes increases facilitative glucose uptake and GLUT2 expression at the rat proximal tubule brush border membrane. *The Journal of Physiology*, *553*(Pt 1), 137–145. https://doi.org/10.1113/jphysiol.2003.046268

McNab, B. K. (1973). Energetics and the Distribution of Vampires. *Journal of Mammalogy*, *54*(1), 131–144. https://doi.org/10.2307/1378876

Miller-Butterworth, C. M., Murphy, W. J., O'Brien, S. J., Jacobs, D. S., Springer, M. S., & Teeling, E. C. (2007). A Family Matter: Conclusive Resolution of the Taxonomic Position of the Long-Fingered Bats, Miniopterus. *Molecular Biology and Evolution*, *24*(7), 1553–1561. https://doi.org/10.1093/molbev/msm076

Muchhala, N., & Serrano, D. (2015). The Complexity of Background Clutter Affects Nectar Bat Use of Flower Odor and Shape Cues. *PLOS ONE*, *10*(10), e0136657. https://doi.org/10.1371/journal.pone.0136657

Murrell, B., Wertheim, J. O., Moola, S., Weighill, T., Scheffler, K., & Pond, S. L. K. (2012). Detecting Individual Sites Subject to Episodic Diversifying Selection. *PLOS Genetics*, *8*(7), e1002764. https://doi.org/10.1371/journal.pgen.1002764

Navale, A. M., & Paranjape, A. N. (2016). Glucose transporters: Physiological and pathological roles. *Biophysical Reviews*, *8*(1), 5–9. https://doi.org/10.1007/s12551-015-0186-2

Neuweiler, G. (2000). *The biology of bats*. New York: Oxford University Press.

Ortega-García, S., Saldaña-Vázquez, R. A., Ortega-García, S., & Saldaña-Vázquez, R. A. (2022). Synthesis of knowledge of the plant diet of nectar-feeding bats of México. *Therya*, *13*(3), 335–343. https://doi.org/10.12933/therya-22-1165

Pagel, M. (1999). Inferring the historical patterns of biological evolution. *Nature*, *401*(6756), 877–884. https://doi.org/10.1038/44766

Paradis, E., & Schliep, K. (2018). ape 5.0: An environment for modern phylogenetics and evolutionary analyses in R. *Bioinformatics*, *35*(3), 526–528. https://doi.org/10.1093/bioinformatics/bty633

Park, H., & Hall, R. (1951). The Gross Anatomy of the Tongues and Stomachs of Eight New World Bats. *Transactions of the Kansas Academy of Science*, *54*(1), 64–72. https://doi.org/10.2307/3626255

Peng, X., He, X., Liu, Q., Sun, Y., Liu, H., Zhang, Q., Liang, J., Peng, Z., Liu, Z., & Zhang, L. (2017). Flight is the key to postprandial blood glucose balance in the fruit bats Eonycteris spelaea and Cynopterus sphinx. *Ecology and Evolution*, *7*(21), 8804–8811. https://doi.org/10.1002/ece3.3416

Pennell, M. W., Eastman, J. M., Slater, G. J., Brown, J. W., Uyeda, J. C., FitzJohn, R. G., Alfaro, M. E., & Harmon, L. J. (2014). geiger v2.0: An expanded suite of methods for fitting macroevolutionary models to phylogenetic trees. *Bioinformatics (Oxford, England)*, *30*(15), 2216–2218. https://doi.org/10.1093/bioinformatics/btu181

Pond, S. L. K., Frost, S. D. W., & Muse, S. V. (2005). HyPhy: Hypothesis testing using phylogenies. *Bioinformatics*, *21*(5), 676–679. https://doi.org/10.1093/bioinformatics/bti079

Pond, S. L. K., Poon, A. F. Y., Velazquez, R., Weaver, S., Hepler, N. L., Murrell, B., Shank, S. D., Magalis, B. R., Bouvier, D., Nekrutenko, A., Wisotsky, S., Spielman, S. J., Frost, S. D. W., & Muse, S. V. (2020). HyPhy 2.5—A Customizable Platform for Evolutionary Hypothesis Testing Using Phylogenies. *Molecular Biology and Evolution*, *37*(1), 295–299. https://doi.org/10.1093/molbev/msz197

Potter, J. H. T., Davies, K. T. J., Yohe, L. R., Sanchez, M. K. R., Rengifo, E. M., Struebig, M., Warren, K., Tsagkogeorga, G., Lim, B. K., dos Reis, M., Dávalos, L. M., & Rossiter, S. J. (2021). Dietary Diversification and Specialization in Neotropical Bats Facilitated by Early Molecular Evolution. *Molecular Biology and Evolution*, *38*(9), 3864–3883. https://doi.org/10.1093/molbev/msab028

Price, E. R., Brun, A., Caviedes-Vidal, E., & Karasov, W. H. (2015). Digestive Adaptations of Aerial Lifestyles. *Physiology*, *30*(1), 69–78. https://doi.org/10.1152/physiol.00020.2014

Protzek, A. O. P., Rafacho, A., Viscelli, B. A., Bosqueiro, J. R., Cappelli, A. P., Paula, F. M. M., Boschero, A. C., & Pinheiro, E. C. (2010). Insulin and glucose sensitivity, insulin secretion and β-cell distribution in endocrine pancreas of the fruit bat Artibeus lituratus. *Comparative Biochemistry and Physiology Part A: Molecular & Integrative Physiology*, *157*(2), 142–148. https://doi.org/10.1016/j.cbpa.2010.05.016

R Core Team. (2019). *R: A Language and Environment for Statistical Computing*. R Foundation for Statistical Computing. https://www.R-project.org/

Revell, L. J. (2012). phytools: An R package for phylogenetic comparative biology (and other things). *Methods in Ecology and Evolution*, *3*(2), 217–223. https://doi.org/10.1111/j.2041-210X.2011.00169.x

Riesenfeld, G., Sklan, D., Bar, A., Eisner, U., & Hurwitz, S. (1980). Glucose absorption and starch digestion in the intestine of the chicken. *The Journal of Nutrition*, *110*(1), 117–121. https://doi.org/10.1093/jn/110.1.117

Ripperger, S. P., & Carter, G. G. (2021). Social foraging in vampire bats is predicted by long-term cooperative relationships. *PLOS Biology*, *19*(9), e3001366. https://doi.org/10.1371/journal.pbio.3001366

Rojas, D., Vale, A., Ferrero, V., & Navarro, L. (2011). When did plants become important to leaf-nosed bats? Diversification of feeding habits in the family Phyllostomidae. *Molecular Ecology*. https://doi.org/10.1111/j.1365-294X.2011.05082.x

Rojas, D., Warsi, O., & Davalos, L. (2016). Bats (Chiroptera: Noctilionoidea) Challenge a Recent Origin of Extant Neotropical Diversity. *Systematic Biology*, *65*. https://doi.org/10.1093/sysbio/syw011

Ross, G., & Holderied, M. W. (2013). Learning and memory in bats: A case study on object discrimination in flower-visiting bats. In *Bat evolution, ecology, and conservation* (pp. 207–224). Springer.

Santana, S. E., Strait, S., & Dumont, E. R. (2011). The better to eat you with: Functional correlates of tooth structure in bats. *Functional Ecology*, *25*(4), 839–847. https://doi.org/10.1111/j.1365-2435.2011.01832.x

Santos, M., Aguirre, L. F., Vázquez, L. B., & Ortega, J. (2003). Phyllostomus hastatus. *Mammalian Species*. https://doi.org/10.1644/0.722.1

Schindelin, J., Arganda-Carreras, I., Frise, E., Kaynig, V., Longair, M., Pietzsch, T., Preibisch, S., Rueden, C., Saalfeld, S., Schmid, B., Tinevez, J.-Y., White, D. J., Hartenstein, V., Eliceiri, K., Tomancak, P., & Cardona, A. (2012). Fiji: An open-source platform for biological-image analysis. *Nature Methods*, *9*(7), 676–682. https://doi.org/10.1038/nmeth.2019

Schondube, J. E., Herrera-M, L. G., & Martínez Del Rio, C. (2001). Diet and the evolution of digestion and renal function in phyllostomid bats. *Zoology*, *104*(1), 59–73. https://doi.org/10.1078/0944-2006-00007

Scillitani, G., Zizza, S., Liquori, G. E., & Ferri, D. (2007). Lectin histochemistry of gastrointestinal glycoconjugates in the greater horseshoe bat, Rhinolophus ferrumequinum (Schreber, 1774). *Acta Histochemica*, *109*(5), 347–357. https://doi.org/10.1016/j.acthis.2007.02.010

Silva, C., Amarante, M., Cordero Schmidt, E., Vargas-Mena, J., Barros, M., Rodrigues Sartori, S., & Barbosa Morais, D. (2020). Comparative Study on the Small and Large Intestines of the Bats Artibeus planirostris and Diphylla ecaudata: Influence of Food Habits on Morphological Parameters. *Acta Chiropterologica*, *22*, 435–448. https://doi.org/10.3161/15081109ACC2020.22.2.016

Smith, M. D., Wertheim, J. O., Weaver, S., Murrell, B., Scheffler, K., & Kosakovsky Pond, S. L. (2015). Less Is More: An Adaptive Branch-Site Random Effects Model for Efficient Detection of Episodic Diversifying Selection. *Molecular Biology and Evolution*, *32*(5), 1342–1353. https://doi.org/10.1093/molbev/msv022

Spoor, S., Cheng, C.-H., Sanderson, L.-A., Condon, B., Almsaeed, A., Chen, M., Bretaudeau, A., Rasche, H., Jung, S., Main, D., Bett, K., Staton, M., Wegrzyn, J. L., Feltus, F. A., & Ficklin, S. P. (2019). Tripal v3: An ontology-based toolkit for construction of FAIR biological community databases. *Database: The Journal of Biological Databases and Curation*, *2019*, baz077. https://doi.org/10.1093/database/baz077

Strobel, S., Encarnação, J. A., Becker, N. I., & Trenczek, T. E. (2015). Histological and Histochemical Analysis of the Gastrointestinal Tract of the Common Pipistrelle Bat (Pipistrellus Pipistrellus). *European Journal of Histochemistry : EJH*, *59*(2), 2477. https://doi.org/10.4081/ejh.2015.2477

Suarez, R. K., & Welch, K. C. (2017). Sugar Metabolism in Hummingbirds and Nectar Bats. *Nutrients*, *9*(7), 743. https://doi.org/10.3390/nu9070743

Symonds, M. R. E., & Blomberg, S. P. (2014). A Primer on Phylogenetic Generalised Least Squares. In L. Z. Garamszegi (Ed.), *Modern Phylogenetic Comparative Methods and Their Application*

in Evolutionary Biology (pp. 105–130). Springer Berlin Heidelberg. https://doi.org/10.1007/978-3-662-43550-2_5

Tobin, V., Le Gall, M., Fioramonti, X., Stolarczyk, E., Blazquez, A. G., Klein, C., Prigent, M., Serradas, P., Cuif, M.-H., Magnan, C., Leturque, A., & Brot-Laroche, E. (2008). Insulin Internalizes GLUT2 in the Enterocytes of Healthy but Not Insulin-Resistant Mice. *Diabetes*, *57*(3), 555–562. https://doi.org/10.2337/db07-0928

UniProt consortium. (2020). UniProt: The universal protein knowledgebase in 2021. *Nucleic Acids Research*, *49*(D1), D480–D489. https://doi.org/10.1093/nar/gkaa1100

Upham, N. S., Esselstyn, J. A., & Jetz, W. (2019). Inferring the mammal tree: Species-level sets of phylogenies for questions in ecology, evolution, and conservation. *PLOS Biology*, *17*(12), e3000494. https://doi.org/10.1371/journal.pbio.3000494

Voigt, C. (2003). Reproductive energetics of the nectar-feeding bat Glossophaga soricina (Phyllostomidae) J. *Journal of Comparative Physiology. B, Biochemical, Systemic, and Environmental Physiology*, *173*, 79–85. https://doi.org/10.1007/s00360-002-0316-6

Voigt, C. C., & Speakman, J. R. (2007). Nectar-feeding bats fuel their high metabolism directly with exogenous carbohydrates. *Functional Ecology*, *21*(5), 913–921. https://doi.org/10.1111/j.1365-2435.2007.01321.x

Voigt, C. C., & Winter, Y. (1999). Energetic cost of hovering flight in nectar-feeding bats (Phyllostomidae: Glossophaginae) and its scaling in moths, birds and bats. *J Comp Physiol B*, *169*(38–48). https://doi.org/10.1007/s003600050191

Walton, K. D., Mishkind, D., Riddle, M. R., Tabin, C. J., & Gumucio, D. L. (2018). Blueprint for an Intestinal Villus: Species-specific Assembly Required. *Wiley Interdisciplinary Reviews. Developmental Biology*, *7*(4), e317. https://doi.org/10.1002/wdev.317

Welch Jr, K. C., Herrera M, L. G., & Suarez, R. K. (2008). Dietary sugar as a direct fuel for flight in the nectarivorous bat Glossophaga soricina. *Journal of Experimental Biology*, *211*(3), 310-316.

Welch, K. C., & Chen, C. C. (2014). Sugar flux through the flight muscles of hovering vertebrate nectarivores: a review. *Journal of Comparative Physiology B*, *184*, 945-959.

Winter, Y., & Stich, K. P. (2005). Foraging in a complex naturalistic environment: Capacity of spatial working memory in flower bats. *Journal of Experimental Biology*, *208*(3), 539–548. https://doi.org/10.1242/jeb.01416

Wright, E. M., Sala-Rabanal, M., Ghezzi, C., & Loo, D. D. F. (2018). Sugar Absorption. In *Physiology of the Gastrointestinal Tract, Sixth Edition* (pp. 1051–1062). Elsevier. https://doi.org/10.1016/B978-0-12-809954-4.00046-3

Wyatt, G. R., & Kalf, G. F. (1957). THE CHEMISTRY OF INSECT HEMOLYMPH. *The Journal of General Physiology*, *40*(6), 833–847.

Yasutake, H., Goda, T., & Takase, S. (1995). Dietary regulation of sucrase-isomaltase gene expression in rat jejunum. *Biochimica et Biophysica Acta (BBA) - General Subjects*, *1243*(2), 270–276. https://doi.org/10.1016/0304-4165(94)00143-L

York, H. A., & Billings, S. A. (2009). Stable-isotope Analysis of Diets of Short-tailed Fruit Bats (Chiroptera: Phyllostomidae: Carollia). *Journal of Mammalogy*, *90*(6), 1469–1477. https://doi.org/10.1644/08-MAMM-A-382R.1

Zepeda Mendoza, M. L., Xiong, Z., Escalera-Zamudio, M., Runge, A. K., Thézé, J., Streicker, D., Frank, H. K., Loza-Rubio, E., Liu, S., Ryder, O. A., Samaniego Castruita, J. A., Katzourakis, A., Pacheco, G., Taboada, B., Löber, U., Pybus, O. G., Li, Y., Rojas-Anaya, E., Bohmann, K., … Gilbert, M. P. T. (2018). Hologenomic adaptations underlying the evolution of sanguivory in the common vampire bat. *Nature Ecology & Evolution*, *2*(4), 659–668. https://doi.org/10.1038/s41559-018-0476-8

Supplemental information

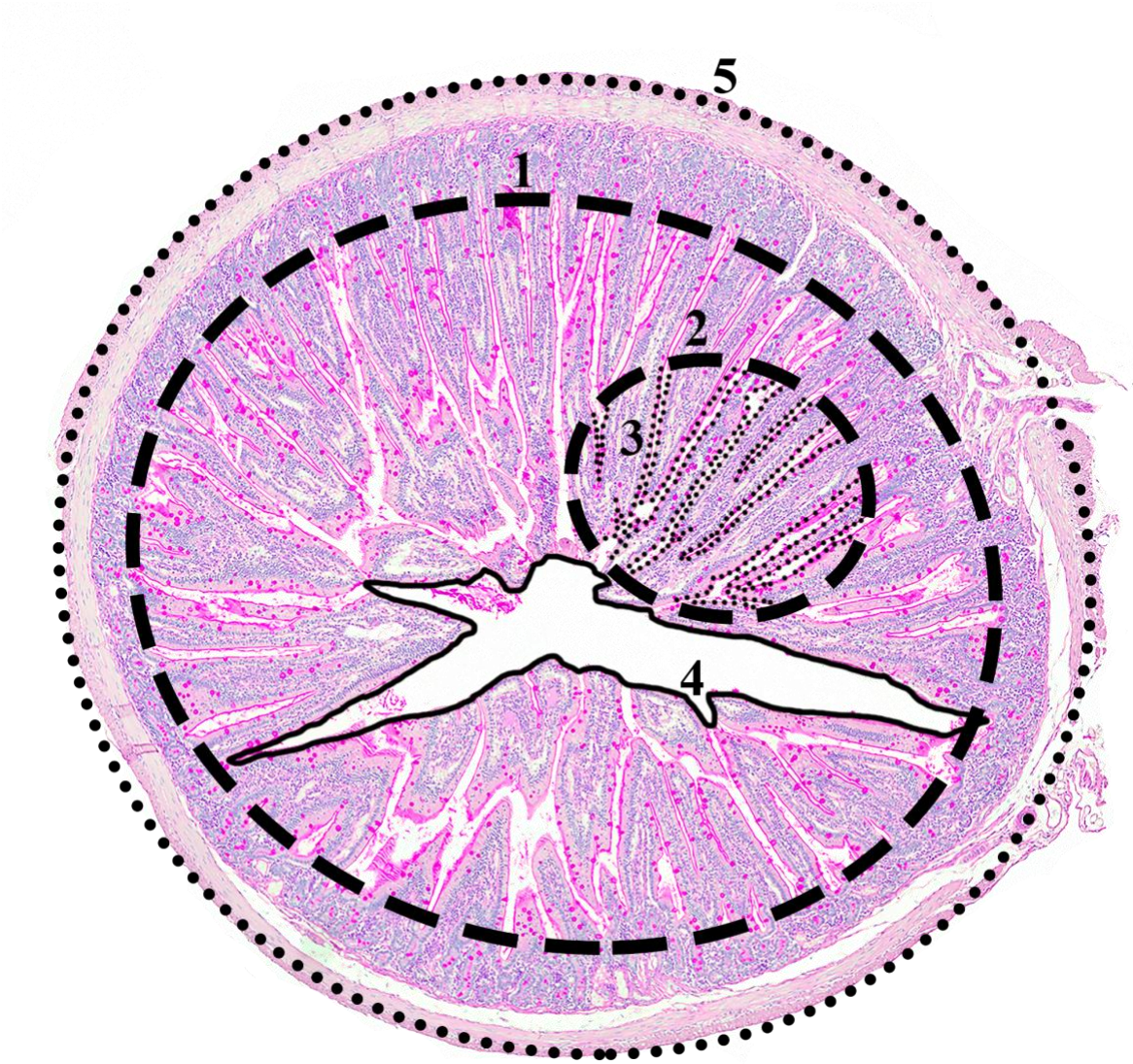

Supplemental Figure 1. Measures extracted from the intestine cross sections. 1. Villi-lumen area (VLA); 2. Sample area (SA); 3. Villi perimeter in the sampled area (VPSA); 4. Lumen area (LA); 5. Cross section perimeter (CSP).

Supplemental Figure 2. Change in blood glucose levels 10-minutes after eating a 20% glucose solution. Each bat was fed a single dose of glucose (5.4mg/kg body weight) after fasting. *Carollia perspicillata*, Seba's short-tailed fruit bat (n=4) increased on average by 446.5mg/dl. *Glossophaga soricina*, Pallas's long-tongued bat (n=4) increased on average by 617.5mg/dl. *Pteronotus parnellii*, Parnell's mustached bat (n=4) increased by average by 184.25mg/dl.

Species	ID	Blood glucose (mg/dl) (t=0)	Blood glucose (mg/dl) (t=10)
Carollia perspicillata	TT22- 01	75	424
	TT22-45	60	538
	TT22-02	70	606
	TT22-03	97	520
Glossophaga soricina	TT22- 37	91	626
	TT22-10	47	683
	TT22-43	36	687
	TT22-52	59	707
Pteronotus parnellii	TT22-19	57	276
	TT22-20	59	241
	TT22-21	95	211
	TT22-22	156	376

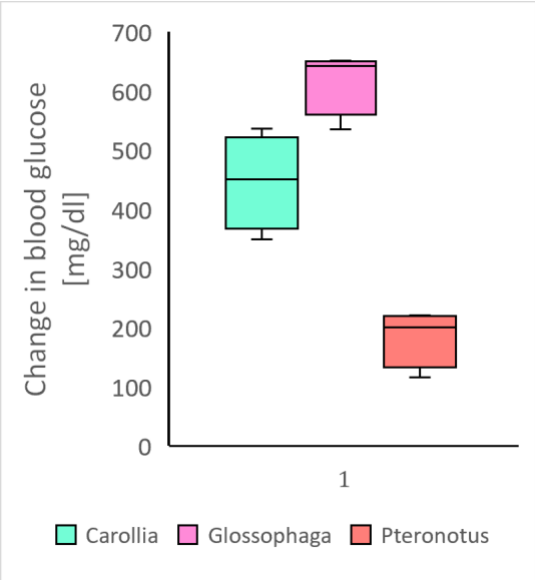

Supplemental Table 1. Species included in the *in vivo* physiology essay. *A. lit: Artibeus lituratus, A. pla: Artibeus planirostris, A. aeq: Artibeus aequatorialis, D. pha: Dermanura phaeotis, U. con: Uroderma convexum, U. bak: Uroderma bakeri, P. hel: Platyrrhinus helleri, S. gia: Sturnira giannae, S. lud: Sturnira ludovici, S. lui: Sturnira luisi, S. par: Sturnira parvidens, G. sor: Glossophaga soricina, C. god: Choeroniscu godmani, C. cas: carollia castanea, C. per: Carollia perspicillata, C. bre: Carollia brevicauda, P. dis: Phyllostomus discolor, P. has: Phyllostomus hastatus, V. spe: Vampyrum spectrum, D. rot: Desmodus rotundus, G. cre: Gardnerycteris crenulatum, M. cau: Myotis caucensis, M. alb: Myotis albescens, M. mol: Molossus molossus, S. bil: Saccopteryx billineata, P. kap: Peropteryx kappleri.*

Family	**Genus**	**Food preference**	**Sugar**	**# Individuals**	**Species**
Phyllostomidae	*Artibeus*	Fruits	Trehalose	17	*A. lit, A. pla, A. aeq*
			Sucrose	22	
			Glucose	13	
	Dermanura		Trehalose	6	*D. pha*
			Sucrose	6	
			Glucose	6	
	Uroderma		Trehalose	1	

			Sucrose	1	*U. con, U. bak*
			Glucose	1	
	Platyrrhinus		Sucrose	1	*P. hel*
	Sturnira		Trehalose	1	*S. gia, S. lud, S. lui, S. par*
			Sucrose	1	
			Glucose	3	
	Glossophaga	Nectar	Trehalose	4	*G. sor*
			Sucrose	6	
			Glucose	4	
	Choeroniscus		Trehalose	1	*C. god*
			Sucrose	1	
			Glucose	2	
	Carollia	Fruits & Insects	Trehalose	18	*C. cas, C. per, C. bre*
			Sucrose	19	
			Glucose	13	
	Phyllostomus	Insects, Nectar, Polen, Fruits, Vertebrates	Trehalose	3	*P. dis, P. has*
			Sucrose	1	
			Glucose	1	
	Vampyrum	Vertebrates	Glucose	1	*V. spe*
	Desmodus	Blood	Trehalose	4	*D.rot*
			Sucrose	4	
			Glucose	6	
	Gardnerycteris	Insects	Trehalose	1	*G. cre*
Mormoopidae	*Pteronotus*		Glucose	12	*P. par*
Vespertilionidae	*Myotis*		Trehalose	3	*M. cau, M. alb*
			Sucrose	1	
			Glucose	2	
Molossidae	*Molossus*		Trehalose	1	*M. mol*
			Glucose	1	
Emballonuridae	*Saccopteryx*		Trehalose	1	*S. bil*
			Sucrose	1	

			Glucose	1	
	Peropteryx		Sucrose	3	*P. kap*
Total				**194**	**27**

Supplemental Table 2. A. phylogenetic signal evaluated for the assimilation of glucose, sucrose and trehalose in Neotropical bats, pattern of assimilation value shown as the 10-60 min measurement. B. PGLS analysis results for the assimilation of sugars by Neotropical bats with BM and Pagel models.

A. Phylogenetic signal			
Sugar	**Variable**	**Lambda (λ)**	**P-value**
Glucose	Measure 10 min	0,518074	0,158051
	Measure 60 min	6,6107e-05	1
	Measure 10-60 min	0,4215	0,251434
Sucrose	Measure 10 min	**0,80632**	**0,00975108**
	Measure 60 min	6,6107e-05	1
	Measure 10-60 min	**0,927203**	**0,0311926**
Trehalose	Measure 10 min	0,717598	0,253792
	Measure 60 min	**0,85204**	**0,0444046**
	Measure 10-60 min	**0,999934**	**0,0210185**
B. PGLS analysis (ML)			
Glucose			

Model	AIC	Delta AIC	AIC wt	Res.LL
BM glucose null	297,02	53,29	0	-146,18
BM glucose~diet	**243,74**	0	1	-110,56
BM sucrose null	233,67	32,93	0	-114,48
BM sucrose~diet	**200,74**	0	1	-91,14
BM trehalose null	193,55	24,72	0	-94,72
BM trehalose~diet	**168,82**	0	1	-75,18

Supplemental Table 3. Candidate genes. All candidate genes were evaluated for episodic positive selection. For relevance to dietary evolution, the main glucose transporters and digestive enzymes were screened for biased function and expression in the duodenum using mouse ENCODE (NCBI Bioproject PRJNA66167) and human HPA (NCBI Bioproject PRJEB4337).

Gene symbol	Other name	Function	Tissue localization	Biased expression
SLC2A1	GLUT-1	Glucose transporter	most cells	
SLC2A2	GLUT-2	Glucose transporter	liver, intestine, hypothalamus, pancreatic beta cells	Duodenum
SLC2A3	GLUT-3	Glucose transporter	insulin-independent in neurons	
SLC2A4	GLUT-4	Glucose transporter	heart, muscle, fat, activated by insulin	
SLC2A5	GLUT-5	Fructose transporter	mucosal surface of small intestine, liver, kidney, testis	Duodenum
SLC5A1	SGLT1	Sodium/glucose cotransporter	mucosal surface of small intestine, kidney cells	Duodenum
SI		Enzyme: sucrase-isomaltase	Brush-border of enterocyte	Duodenum
TREH		Enzyme: trehalase	Brush-border of enterocyte	Duodenum

Supplemental Table 4. Example of single orthologs identified using OMA groups.

Gene Symbol	HGNC	OMA April 2021 ID			
		HUMAN	**MYOLU**	**PTEVA**	**SORAR**
SI	HGNC:10856	HUMAN73257	MYOLU05002	PTEVA09730	
SLC2A1	HGNC:11005	HUMAN49272	MYOLU04066	PTEVA06559	
SLC2A2	HGNC:11006	HUMAN73390	MYOLU04971	PTEVA03338	SORAR12909
SLC2A3	HGNC:11007	HUMAN10977			
SLC2A4	HGNC:11009	HUMAN31341	MYOLU16326	PTEVA10146	SORAR11731
SLC2A5	HGNC:11010	HUMAN47323		PTEVA04335	
SLC5A1	HGNC:11036	HUMAN60154	MYOLU14967	PTEVA05350	SORAR08074
TREH	HGNC:12266	HUMAN09727	MYOLU19227	PTEVA02820	SORAR02542

Supplemental Table 5. Twenty-two bat genomes were assembled and annotated for selection tests. Species were selected to best match the diversity of the *in vivo* physiology data. Two outgroup genomes, human and shrew, were used to polarize the evolutionary changes in bats.

Family	Species	Year published	NCBI accession	RNAseq/ Proteome	Species Code
Vespertilionidae	*Eptesicus fuscus*	2020	*DNAzoo SRS7189612	GCF_000308155.1	EFU
Vespertilionidae	*Myotis myotis*	2020	GCA_014108235.1	GCF_014108235.1	MMY
Vespertilionidae	*Myotis septentrionalis*	2020	*DNAzoo SRS7189622	Hi-C	MSE
Molossidae	*Molossus molossus*	2020	GCA_014108415.1	GCF_014108415.1, SRR9703456	MMO
Miniopteridae	*Miniopterus natalensis*	2016	GCA_001595765.1	GCF_001595765.1	MNA

Miniopteridae	*Miniopterus schreibersii*	2019	GCA_004026525.1	n/a	MSC
Mormoopidae	*Pteronotus parnellii*	2013	GCA_000465405.1	SRR9703452, PRJNA481095, PRJNA481095	PPA
Mormoopidae	*Mormoops blainvillei*	2019	GCA_004026545.1	SRR9703451	MBL
Phyllostomidae	*Desmodus rotundus*	2018	GCA_002940915.1	GCF_002940915.1, SRR9703482, PRJNA178123, SRR8878915	DRO
Phyllostomidae	*Anoura caudifer*	2019	GCA_004027475.1	SRR9703485	ACA
Phyllostomidae	*Musonycteris harrisonii*	2021	*Gigadb 100746	n/a	MHA
Phyllostomidae	*Leptonycteris nivalis*	2020	PRJNA543656	n/a	LNI
Phyllostomidae	*Leptonycteris yerbabuenae*	2020	PRJNA627035	SRR9087861, SRR9087862, SRR9087863, SRR9087864	LYE
Phyllostomidae	*Macrotus waterhousii*	2020	*Gigadb 100746	SRR9703483	MWA
Phyllostomidae	*Macrotus californicus*	2019	GCA_007922815.1	n/a	MCA
Phyllostomidae	*Micronycteris hirsuta*	2019	GCA_004026765.1	n/a	MHI

Phyllostomidae	*Tonatia saurophila*	2019	GCA_004024845.1	n/a	TSA
Phyllostomidae	*Phyllostomus discolor*	2019	GCA_004126475.2	GCF_004126475.2	PDI
Phyllostomidae	*Phyllostomus hastatus*	2021	GCA_019186645.1	SRR9703480	PHA
Phyllostomidae	*Sturnira hondurensis*	2020	GCA_014824575.2	GCF_014824575.2	SHO
Phyllostomidae	*Carollia perspicillata*	2019	GCA_004027735.1	SRR9703464, SRR5872538	CPE
Phyllostomidae	*Artibeus jamaicensis*	2019	GCA_004027435.1	SRR9703479, SRR539297, PRJNA305413	AJA
Primates	*Homo sapiens*	2019	GCA_000001405.28	GCF_000001405.39	HSA
Eulipotyphla	*Sorex araneus*	2012	GCA_000181275.2	n/a	SAR

Supplemental Table 6. Statistical summary of the exploratory aBSREL results. aBSREL (adaptive Branch-Site Random Effects Likelihood) will test whether a proportion of sites have evolved under positive selection along each branch in the phylogeny. Baseline model refers to MG94xREV baseline model that infers a single omega rate per branch. Full adaptive model infers an optimized number of omega rate categories per branch. After aBSREL fits the full adaptive model, the Likelihood Ratio Test (LRT) is performed at each branch and compares the full model to a null model where branches are not allowed to have rate classes of $\omega>1$.

Gene	aBSREL Model	AIC_C	logL	Parameters
SLC2A1	Nucleotide GTR	32127.80	-16014.83	49

	Baseline	30189.65	-15002.06	92
	Full adaptive model	29812.02	-14805.10	100
SLC2A2	Nucleotide GTR	74075.49	-36984.67	53
	Baseline	72399.71	-36117.31	82
	Full adaptive model	72101.26	-35951.86	98
SLC2A3	Nucleotide GTR	44911.77	-22402.81	53
	Baseline	43351.46	-21574.92	100
	Full adaptive model	42565.78	-21153.57	128
SLC2A4	Nucleotide GTR	49387.03	-24640.44	53
	Baseline	47689.57	-23744.00	100
	Full adaptive model	47653.74	-23724.05	102
SLC2A5	Nucleotide GTR	49623.49	-24760.68	51
	Baseline	46931.60	-23379.26	86
	Full adaptive model	46529.65	-23158.00	106
SLC5A1	Nucleotide GTR	93090.21	-46494.05	51
	Baseline	89484.54	-44653.76	88
	Full adaptive model	88528.46	-44155.46	108
SI	Nucleotide GTR	195876.34	-97887.15	51
	Baseline	191316.64	-95568.12	90
	Full adaptive model	189682.39	-94710.79	130
TREH	Nucleotide GTR	14800.36	-7375.14	25

	Baseline	14468.32	-7185.76	48
	Full adaptive model	14453.92	-7174.49	52

Supplemental Table 7. Detailed aBSREL significant results in bats. The results are from exploratory analysis where all branches are tested for positive selection. In this scenario, p-values at each branch must be corrected for multiple testing (using the Holm-Bonferroni correction). The Likelihood Ratio Test (LRT) is performed at each branch and compares the full model to a null model where branches are not allowed to have rate classes of ω>1. Branches and nodes under selection are shown below and correspond to **Figure 4.**

Gene	Branch	LRT	p-value	ω distribution
SLC2A1	ACA	170.2147	<0.0001	ω_1= 0.00 (35%) ω_2= 9090 (65%)
	Node 30	13.0492	0.0005	ω_1= 0.00 (99%) ω_2= 111 (0.54%)
SLC2A2	ACA	30.9776	<0.0001	ω_1= 1.00 (37%) ω_2= 334 (63%)
	MHA	64.2921	<0.0001	ω_1= 1.00 (20%) ω_2= 1e5 (80%)
	Node 13	35.4885	<0.0001	ω_1= 0.00 (33%) ω_2= 1e5 (67%)
	MMY	19.7098	<0.0001	ω_1= 0.794 (12%) ω_2= 80.6 (88%)
SLC2A3	DRO	30.6385	<0.0001	ω_1= 0.104 (98%) ω_2= 247 (1.9%)
	MSE	302.4789	<0.0001	ω_1= 0.00 (46%) ω_2= 868 (54%)
	Node 10	39.5755	<0.0001	ω_1= 0.272 (98%) ω_2= 1e5 (1.7%)
	Node 36	29.7309	<0.0001	ω_1= 0.00 (90%) ω_2=11.6 (9.6%)
	SAR	15.3250	0.0002	ω_1= 0. (72%) ω_2= 0.611 (14%) ω_3= 1e5 (13%)
	Node 37	13.3182	0.0004	ω_1= 0.374 (99%) ω_2= 158 (0.67%)

SLC2A4	n/a	n/a	n/a	n/a
SLC2A5	EFU	28.7577	<0.0001	ω_1= 0.243 (11%) ω_2= 13.9 (89%)
	MSE	15.5125	0.0001	ω_1= 0.351 (93%) ω_2= 1e5 (6.7%)
	Node 39	12.1544	0.0008	ω_1= 0.024 (3.7%) ω_2= 13.2 (96%)
SLC5A1	MNA	447.4476	<0.0001	ω_1= 0.0776 (90%) ω_2=100000 (10%)
	TSA	16.1794	0.0001	ω_1= 1e9 (100%)
SI	MNA	96.3819	<0.0001	ω_1= 1.00 (98%) ω_2= 1.00 (1.8%) ω_3= 1e5 (0.60%)
	MSC	53.7631	<0.0001	ω_1= 0.301 (99%) ω_2= 6250 (0.5%)
	MWA	27.5404	<0.0001	ω_1= 0.00 (2.9%) ω_2= 1e5 (97%)
	Node 34	45.6658	<0.0001	ω_1= 1.00 (6.3%) ω_2= 9090 (94%)
	Node 39	38.1848	<0.0001	ω_1= 0.215 (97%) ω_2= 40.7 (3.1%)
	PHA	49.2379	<0.0001	ω_1= 1.00 (3.9%) ω_2= 3850 (96%)
	MSE	20.0862	<0.0001	ω_1= 0.200 (5%) ω_2= 1e5 (95%)
	Node 10	17.5613	0.0001	ω_1= 0.00 (92%) ω_2= 7.81 (8%)
TREH	Node 11	22.4132	<0.0001	ω_1= 3.77 (100%)
	EFU	0.0221	0.0014	ω_1= 0.00 (78%) ω_2= 13.2 (22%)